Icarus **155**, 436–453 (2002)
doi:10.1006/icar.2001.6741, available online at http://www.idealibrary.com on IDEAL®

Evolution of Planetesimal Velocities Based on Three-Body Orbital Integrations and Growth of Protoplanets

Keiji Ohtsuki and Glen R. Stewart

Laboratory for Atmospheric and Space Physics, University of Colorado, 392 UCB, Boulder, Colorado 80309-0392
E-mail: ohtsuki@lasp.colorado.edu

and

Shigeru Ida

Department of Earth and Planetary Sciences, Tokyo Institute of Technology, Tokyo 152-8551, Japan

Received June 21, 2001; revised August 8, 2001

We obtain the viscous stirring and dynamical friction rates of planetesimals with a Rayleigh distribution of eccentricities and inclinations, using three-body orbital integration and the procedure described by Ohtsuki (1999, *Icarus* 137, 152), who evaluated these rates for ring particles. We find that these rates based on orbital integrations agree quite well with the analytic results of Stewart and Ida (2000, Icarus 143, 28) in high-velocity cases. In low-velocity cases where Kepler shear dominates the relative velocity, however, the three-body calculations show significant deviation from the formulas of Stewart and Ida, who did not investigate the rates for low velocities in detail but just presented a simple interpolation formula between their high-velocity formula and the numerical results for circular orbits. We calculate evolution of root mean square eccentricities and inclinations using the above stirring rates based on orbital integrations, and find excellent agreement with *N*-body simulations for both one- and two-component systems, even in the low-velocity cases. We derive semi-analytic formulas for the stirring and dynamical friction rates based on our numerical results, and confirm that they reproduce the results of *N*-body simulations with sufficient accuracy. Using these formulas, we calculate equilibrium velocities of planetesimals with given size distributions. At a stage before the onset of runaway growth of large bodies, the velocity distribution calculated by our new formulas are found to agree quite well with those obtained by using the formulas of Stewart and Ida or Wetherill and Stewart (1993, *Icarus* 106, 190). However, at later stages, we find that the inclinations of small collisional fragments calculated by our new formulas can be much smaller than those calculated by the previously obtained formulas, so that they are more easily accreted by larger bodies in our case. The results essentially support the previous results such as runaway growth of protoplanets, but they could enhance their growth rate by 10–30% after early runaway growth, where those fragments with low random velocities can significantly contribute to rapid growth of runaway bodies.

Key Words: **celestial mechanics; origin, solar system; planetary formation; planetesimals.**

1. INTRODUCTION

In order to study the early stages of planetary accretion from a very large number of planetesimals, numerical simulations based on a coagulation equation are generally used (e.g., Greenberg *et al*. 1978, Nakagawa *et al*. 1983, Ohtsuki *et al*. 1988, Wetherill and Stewart 1989, 1993, Weidenschilling *et al*. 1997, Kenyon and Luu 1998, 1999, Inaba *et al*. 2001, and references therein). In these simulations, planetesimals with broad size distributions are divided into a number of discrete size bins, and the evolution of size distributions is calculated according to the collision rate between each pair of these size bins. Since the accretion rate depends on the mean eccentricity and inclination of planetesimals, it is essential to derive accurate velocity evolution equations that can be used in these simulations.

Mainly two different approaches have been made to derive velocity evolution equations. In one approach, evolution of mean square velocities relative to the local circular velocity is studied using the Fokker–Planck equation and Boltzmann equation (e.g., Stewart and Kaula 1980, Hornung *et al*. 1985, Stewart and Wetherill 1988, Wetherill and Stewart 1993), while orbital elements based on Hill's approximation in the three-body problem are used in another approach (e.g., Ida 1990, Ida *et al*. 1993, Tanaka and Ida 1996). Recently, evolution equations for mean square eccentricity and inclination of particles with the Rayleigh distribution of eccentricities and inclinations have been derived by improving earlier works (Ohtsuki 1999, Stewart and Ida 2000). Stewart and Ida (2000) also demonstrated the equivalence between the equation obtained from the Fokker–Planck equation and the Hill formalism equation. These equations show that the evolution can be calculated if the viscous stirring and dynamical friction rates of eccentricity and inclination are given as a function of mean square eccentricity and inclination (see Section 2).

Ohtsuki (1999, hereafter O99) obtained the viscous stirring and dynamical friction rates for particles in planetary rings with

0019-1035/02 $35.00

low optical depth by three-body orbital integrations. He calculated particle velocity evolution using these stirring rates and the above evolution equation, and found excellent agreement with N-body simulations when the restitution coefficient of particles is sufficiently small to achieve an equilibrium state and the optical depth is sufficiently small to be gravitationally stable (O99, Ohtsuki and Emori 2000).

On the other hand, Stewart and Ida (2000, hereafter SI00) derived analytic formulas of the stirring rates for planetesimals. SI00 compared the velocity evolution calculated by their formulas with N-body simulations, and found fairly good agreement in the cases of relatively high velocities where relative velocities are dominated by random velocities of planetesimals rather than Kepler shear velocities. Inaba *et al*. (2001) carried out numerical simulations of planetary accretion using a coagulation equation and SI00's formulas for velocity evolution. Their results of comparison with N-body simulations showed excellent agreement, further supporting the relevance of SI00's formulas.

However, SI00 did not investigate in detail the velocity stirring rates for low-velocity cases where Kepler shear dominates relative velocities, but presented a simple interpolation formula between their high-velocity formula and the numerical results for circular orbits (Ida 1990). SI00 noted that the velocity evolution obtained by their simple interpolation formula disagrees with N-body simulations in the shear-dominated regime. SI00 also found that the dynamical friction terms in their analytic formulas have to be reduced by 30% to obtain better agreement with N-body simulations. Since the planetesimal velocities in the simulations of Inaba *et al*. (2001) were always relatively high because of their choice of large initial mass of planetesimals ($\gtrsim 10^{23}$ g) and neglect of fragmentation, Inaba *et al*. found good agreement with N-body simulations. More accurate formulas for velocity evolution including low-velocity cases are needed to produce more accurate numerical simulations of planetary accretion with the effect of collisional fragmentation, where small fragments can have much smaller random velocities and accelerate the growth of protoplanets (Wetherill and Stewart 1993). Ida (1990) obtained stirring rates for various pairs of eccentricities and inclinations including low-velocity cases using three-body orbital integrations, but distribution of eccentricities and inclinations was not taken into account. Shiidsuka and Ida (1999) also used three-body orbital integration to obtain the Rayleigh distribution averages of viscous stirring rate for various disk potentials and studied anisotropy of velocity dispersion. However, they didn't derive semi-analytic expression for the viscous stirring rate, and the dynamical friction rate was not calculated as they focused on systems of equal-sized particles.

Wetherill and Stewart (1993, hereafter WS93) took into account the stirring rates due to low-velocity shear-dominated encounters based on the numerical results of Ida (1990). They used the analytic values of the stirring rates derived under the two-body approximation for high-velocity cases and the velocity-dependence of the numerical results of Ida (1990) to obtain the stirring rates in the shear-dominated region. In such low-velocity cases, it is known that the stirring rate of inclinations is much smaller than that of eccentricities (Ida 1990). Therefore, calculating separately the evolution of eccentricity and inclination rather than assuming a fixed ratio of inclination to eccentricity, WS93 took into account the qualitative effects of low-velocity encounters in their simulation of planetesimal accumulation. Their findings include the fact that collisional fragments with low random velocities contribute significantly to the growth of protoplanets after their early runaway growth. The expressions for the stirring rates reported in WS93 have been used also in other later works (e.g., Weidenschilling *et al*. 1997, Kenyon and Luu 1998, 1999). Weidenschilling *et al*. (1997) adopted the WS93's expressions with modifications appropriate for their multizone simulations, including the correction for the treatment of distant encounters (for detail, see their Appendix B). However, as stated in SI00, in high-velocity cases, the rate of viscous stirring and dynamical friction of inclinations as well as the rate of dynamical friction of eccentricities reported in WS93 were a factor of 2 or 4 overestimated compared to more accurate results of SI00. We also find that the rate of viscous stirring of eccentricities in the shear-dominated velocity cases used in WS93 is underestimated compared to the results of three-body orbital integration, because of their simplified method of extrapolation (Section 2.4). Although Inaba *et al*. (2001) confirmed that the correction of the coefficients for the stirring rates in the high-velocity cases causes very little difference in the results of their simulation of planetesimal accumulation, it is desirable to derive more accurate formulas including low-velocity cases, which could affect the growth of protoplanets once fragmentation is taken into account. More recently, Kenyon and Bromley (2001) adopted an approach similar to WS93's by using SI00's formulas for the dispersion-dominated regime, and the formulas for the shear-dominated regime was obtained using the velocity-dependence of the stirring rates found by Ida (1990) with numerical coefficients adjusted to reproduce the results of N-body simulations (Ida and Makino 1992, 1993).

In the present work, we obtain stirring and dynamical friction rates of planetesimals with a Rayleigh distribution of eccentricities and inclinations by three-body orbital integrations for a wide range of parameters, using the method described by Ohtsuki (1999). We find that velocity evolution calculated by these stirring rates reproduces N-body simulations remarkably well even in the case of shear-dominated low velocities. First, in Section 2, we briefly summarize the formulation for the velocity evolution of planetesimals, which will be used in later sections. Then, we present numerical results of stirring rates obtained by three-body orbital integration, both with and without distribution of eccentricities and inclinations. In Section 3, we derive semi-analytic formulas for the stirring rates, using our numerical results and the analytic results of SI00 for high-velocity cases with slight modification. Section 4 is devoted to the discussion of equilibrium velocities of planetesimals with given size distributions. We show that orbital inclinations of small collisional

fragments ($\lesssim 10^{13}$ g) calculated by our new formulas can become significantly smaller than those based on previous works, which could affect the growth rate of protoplanets after early runaway growth. Summary of our results and discussion are presented in Section 5.

2. VISCOUS STIRRING AND DYNAMICAL FRICTION RATES BASED ON THREE-BODY ORBITAL INTEGRATIONS

2.1. Basic Formulation

In the present paper, we describe the evolution of the mean square orbital eccentricities and inclinations using orbital elements of planetesimals based on Hill's approximations (e.g., Ida 1990, O99). One can also derive similar equations for velocity evolution based on the local-velocity formalism (e.g., Stewart and Wetherill 1988), and the translation between the variables in these two approaches is discussed in SI00. We will discuss the relation between the evolution of the mean square velocity relative to the local circular orbit and that of mean square eccentricity and inclination at the end of this section.

We consider gravitational interactions of planetesimals in Hill's coordinates (Hill 1878, Hénon and Petit 1986, Nakazawa and Ida 1988), where the coordinates of the planetesimals are referred to a reference point that moves on a circular orbit with semimajor axis a_0 at the Keplerian angular velocity $\Omega = (GM_\odot/a_0^3)^{1/2}$. A rotating Cartesian coordinate system is erected with origin at the reference position, the x-axis pointing radially outward, the y-axis pointing in the direction of the orbital motion, and the z-axis normal to the equatorial plane. In this case, equations for the motion of the planetesimals relative to the refernece point can be linearized, and they can be written in nondimensional forms if time is scaled by Ω^{-1} and length by the Hill radius $R_H \equiv h_{12}a_0$; h_{12} is defined in terms of the masses of the mutually interacting planetesimals m_1 and m_2 as

$$h_{12} = \left(\frac{m_1 + m_2}{3M_\odot}\right)^{1/3}. \tag{1}$$

In the following, tildes are used to denote scaled quantities. The motion of planetesimal j is then expressed as

$$\begin{aligned} \tilde{x}_j &= \tilde{b}_j - \tilde{e}_j \cos(\tilde{t} - \tau_j), \\ \tilde{y}_j &= -\frac{3}{2}\tilde{b}_j(\tilde{t} - \phi_j) + 2\tilde{e}_j \sin(\tilde{t} - \tau_j), \\ \tilde{z}_j &= \tilde{i}_j \sin(\tilde{t} - \omega_j), \end{aligned} \tag{2}$$

where τ_j and ω_j are the time of perihelion passage (scaled by Ω^{-1}) and argument of perihelion, ϕ_j defines the origin of time, and $\tilde{e}_j$, $\tilde{i}_j$, and $\tilde{b}_j$ are scaled as

$$\begin{aligned} \tilde{e}_j &= e_j/h_{12}, \\ \tilde{i}_j &= i_j/h_{12}, \\ \tilde{b}_j &= (a_j - a_0)/h_{12}a_0. \end{aligned} \tag{3}$$

Furthermore, the motions of the two planetesimals can be separated into the relative motion and the center of mass motion, and the center of mass motion is unaffected by gravitational interactions between planetesimals (Nakazawa and Ida 1988). The nondimensional equations for the relative motion are written as

$$\begin{aligned} \ddot{\tilde{x}} &= 2\dot{\tilde{y}} + 3\tilde{x} - 3\tilde{x}/\tilde{r}^3, \\ \ddot{\tilde{y}} &= -2\dot{\tilde{x}} - 3\tilde{y}/\tilde{r}^3, \\ \ddot{\tilde{z}} &= -\tilde{z} - 3\tilde{z}/\tilde{r}^3, \end{aligned} \tag{4}$$

where $\tilde{r} = (\tilde{x}^2 + \tilde{y}^2 + \tilde{z}^2)^{1/2}$. We can define the orbital elements for the relative motion (Hénon and Petit 1986) as

$$\begin{aligned} (\tilde{e}\cos\tau, \tilde{e}\sin\tau) &\equiv (\tilde{e}_2\cos\tau_2 - \tilde{e}_1\cos\tau_1, \tilde{e}_2\sin\tau_2 - \tilde{e}_1\sin\tau_1), \\ (\tilde{i}\cos\omega, \tilde{i}\sin\omega) &\equiv (\tilde{i}_2\cos\omega_2 - \tilde{i}_1\cos\omega_1, \tilde{i}_2\sin\omega_2 - \tilde{i}_1\sin\omega_1), \\ \tilde{b} &\equiv \tilde{b}_2 - \tilde{b}_1. \end{aligned} \tag{5}$$

Using these variables, we can write the evolution equation for the mean eccentricities and inclinations (O99). For example, in a system of bimodal population of planetesimals with masses m_1 and m_2 the evolution equation for the mean square eccentricities and inclinations of component 1 planetesimals is written as

$$\begin{aligned} \frac{d\langle e_1^2\rangle}{dt} &= a_0^2\Omega \sum_{j=1,2}\left[N_{sj}\frac{h_{1j}^4 m_j}{(m_1+m_j)^2} \right. \\ &\quad \left. \times\left\{m_j\langle P_{VS}\rangle_{1j} + \frac{m_j\langle e_j^2\rangle - m_1\langle e_1^2\rangle}{\langle e_1^2\rangle + \langle e_j^2\rangle}\langle P_{DF}\rangle_{1j}\right\}\right], \\ \frac{d\langle i_1^2\rangle}{dt} &= a_0^2\Omega \sum_{j=1,2}\left[N_{sj}\frac{h_{1j}^4 m_j}{(m_1+m_j)^2} \right. \\ &\quad \left. \times\left\{m_j\langle Q_{VS}\rangle_{1j} + \frac{m_j\langle i_j^2\rangle - m_1\langle i_1^2\rangle}{\langle i_1^2\rangle + \langle i_j^2\rangle}\langle Q_{DF}\rangle_{1j}\right\}\right], \end{aligned} \tag{6}$$

where N_{sj} is the surface number density of component j planetesimals, and

$$h_{1j} = \left(\frac{m_1 + m_j}{3M_\odot}\right)^{1/3}. \tag{7}$$

Furthermore, $\langle P_{VS}\rangle$ and $\langle P_{DF}\rangle$ are the viscous stirring and dynamical friction rates given as a function of scaled eccentricity

and inclination of relative motion as

$$\langle P_{VS}\rangle = \int P_{VS}(\tilde{e},\tilde{i})f(\tilde{e},\tilde{i})\,d\tilde{e}\,d\tilde{i},$$
$$\langle P_{DF}\rangle = \int P_{DF}(\tilde{e},\tilde{i})f(\tilde{e},\tilde{i})\,d\tilde{e}\,d\tilde{i}, \tag{8}$$

where

$$P_{VS}(\tilde{e},\tilde{i}) = \int \Delta\tilde{e}^2\frac{3}{2}|\tilde{b}|\,d\tilde{b}\frac{d\tau\,d\omega}{(2\pi)^2},$$
$$P_{DF}(\tilde{e},\tilde{i}) = -2\tilde{e}\int \Delta\tilde{e}_{\parallel}\frac{3}{2}|\tilde{b}|\,d\tilde{b}\frac{d\tau d\omega}{(2\pi)^2}. \tag{9}$$

The viscous stirring and dynamical friction rates for inclinations ($\langle Q_{VS}\rangle$ and $\langle Q_{DF}\rangle$) are also defined in a similar manner, by substituting $\Delta\tilde{i}^2$ and $\tilde{i}\Delta\tilde{i}_{\parallel}$ for $\Delta\tilde{e}^2$ and $\tilde{e}\Delta\tilde{e}_{\parallel}$ in Eqs. (9). $\Delta\tilde{e}^2$, $\Delta\tilde{e}_{\parallel}$, $\Delta\tilde{i}^2$, and $\Delta\tilde{i}_{\parallel}$ denote the changes caused by each encounter, where $\Delta\tilde{e}_{\parallel}$ and $\Delta\tilde{i}_{\parallel}$ are defined as (Ida 1990)

$$\Delta\tilde{e}_{\parallel} = \cos\tau\cdot\Delta(\tilde{e}\cos\tau) + \sin\tau\cdot\Delta(\tilde{e}\sin\tau),$$
$$\Delta\tilde{i}_{\parallel} = \cos\omega\cdot\Delta(\tilde{i}\cos\omega) + \sin\omega\cdot\Delta(\tilde{i}\sin\omega). \tag{10}$$

The distribution function f is known to follow the Rayleigh distribution function (Ida and Makino 1992, O99) given as

$$f(\tilde{e},\tilde{i}) = \frac{4\tilde{e}\tilde{i}}{\langle\tilde{e}^2\rangle\langle\tilde{i}^2\rangle}\exp\left(-\frac{\tilde{e}^2}{\langle\tilde{e}^2\rangle}-\frac{\tilde{i}^2}{\langle\tilde{i}^2\rangle}\right), \tag{11}$$

with

$$\langle\tilde{e}^2\rangle = \langle\tilde{e}_1^2\rangle + \langle\tilde{e}_2^2\rangle \quad\text{and}\quad \langle\tilde{i}^2\rangle = \langle i_1^2\rangle + \langle\tilde{i}_2^2\rangle. \tag{12}$$

When $j = 1$ on the right-hand side of Eqs. (6), the dynamical friction term vanishes and $\langle P_{VS}\rangle_{11}$ and $\langle Q_{VS}\rangle_{11}$ denote the viscous stirring due to interactions between planetesimals of the same size with $\langle e^2\rangle = 2\langle e_1^2\rangle$ and $\langle i^2\rangle = 2\langle i_1^2\rangle$.

Equations (6) can be also extended to a system of more than two size components. If planetesimals have a continuous size distribution, Eqs. (6) can be rewritten as (O99)

$$\frac{d\langle e_{m_1}^2\rangle}{dt} = a_0^2\Omega\int n_s(m)\frac{h_{m_1,m}^4 m}{(m_1+m)^2}\times\left\{m\langle P_{VS}\rangle_{m_1,m} + \frac{m\langle e_m^2\rangle - m_1\langle e_{m_1}^2\rangle}{\langle e_{m_1}^2\rangle+\langle e_m^2\rangle}\langle P_{DF}\rangle_{m_1,m}\right\}dm,$$
$$\frac{d\langle i_{m_1}^2\rangle}{dt} = a_0^2\Omega\int n_s(m)\frac{h_{m_1,m}^4 m}{(m_1+m)^2}\times\left\{m\langle Q_{VS}\rangle_{m_1,m} + \frac{m\langle i_m^2\rangle - m_1\langle i_{m_1}^2\rangle}{\langle i_{m_1}^2\rangle+\langle i_m^2\rangle}\langle Q_{DF}\rangle_{m_1,m}\right\}dm, \tag{13}$$

where $n_s(m)\,dm$ is the surface number density of planetesimals within the mass range of m to $m+dm$. Equations (6) will be used for the calculations of velocity evolution to compare with N-body simulations in Sections 2.3 and 3. Equations (13) will be used for the calculation of equilibrium velocities of planetesimals with given size distributions in Section 4.

The horizontal and vertical components of the mean square velocity relative to the local circular orbit can be expressed in terms of the mean square eccentricity and inclination as

$$\langle v_{h,m_1}^2\rangle = \frac{5}{8}\langle e_{m_1}^2\rangle v_K^2,$$
$$\langle v_{v,m_1}^2\rangle = \frac{1}{2}\langle i_{m_1}^2\rangle v_K^2, \tag{14}$$

where $v_K = a_0\Omega$ is the circular Keplerian velocity (Lissauer and Stewart 1993). Therefore, using Eqs. (13) (or (6)) with Eqs. (14), one can also obtain the evolution equation for the horizontal component $\langle v_{h,m_1}^2\rangle$ (vertical component $\langle v_{v,m_1}^2\rangle$) of the mean square velocity expressed in terms of $\langle P_{VS}\rangle$ and $\langle P_{DF}\rangle$($\langle Q_{VS}\rangle$ and $\langle Q_{DF}\rangle$).

2.2. Dependence on Eccentricity and Inclination

First, we investigate the dependence of viscous stirring and dynamical friction rates on the eccentricity and inclination for relative motion, using three-body orbital integrations as well as the analytic results for high velocities (Tanaka and Ida 1996). In particular, we examine asymptotic behavior of these rates in both low- and high-velocity limit, which will be used for the calculation of their Rayleigh distribution averages (Section 2.3).

Our numerical methods for three-body orbital integrations are described in our previous papers (Ida 1990, Ohtsuki 1993, Ohtsuki and Ida 1998, O99). In contrast to the calculations for ring particles such as done by O99, here we only calculate orbital changes due to gravitational encounters. The sum of the radii of two interacting planetesimals ($R_{p1}+R_{p2}$) scaled by the Hill radius R_H is given by

$$\tilde{r}_p \equiv \frac{R_{p1}+R_{p2}}{R_H} = \left(\frac{9}{4\pi}\right)^{1/3}\rho_p^{-1/3}a_0^{-1}M_\odot^{1/3}\frac{1+\mu^{1/3}}{(1+\mu)^{1/3}}, \tag{15}$$

where ρ_p is the material density of a planetesimal and $\mu = m_2/m_1$; we have $\tilde{r}_p \simeq 0.005$ when $\rho_p = 3\ \mathrm{g\,cm^{-3}}$, $a_0 = 1\mathrm{AU}$, and $\mu \ll 1$. On the other hand, $\mathcal{O}(\tilde{r}_p)\sim 1$ in planetary rings (O99), where direct collisions play a more important role in the velocity evolution.

Orbital integrations are performed using the eighth-order Runge–Kutta integrator. First, we carry out integrations with rather coarse grids with respect to $\tilde{b}$, τ, and ω for a given pair

of $\tilde{e}$ and $\tilde{i}$, and search for those orbits whose closest approach distance to a planetesimal at the origin $(\tilde{x}, \tilde{y}, \tilde{z}) = (0, 0, 0)$ is less than the Hill radius (i.e., $\tilde{r}_{\rm min} \leq 1$). Next, we choose $\tilde{b}$, τ, and ω with finer grids around the values for those orbits with $\tilde{r}_{\rm min} \leq 1$, and integrate only those orbits, using a smaller target size $\tilde{r}_{\rm min}$ (10^{5-6} orbits are integrated for given $\tilde{e}$, $\tilde{i}$, and $\tilde{r}_{\rm min}$). We repeat this procedure several times until we find a sufficiently large number ($\gtrsim 10^4$) of orbits that satisfy $\tilde{r}_{\rm min} \leq 0.005$ for a given pair of $\tilde{e}$ and $\tilde{i}$. Finally, using Eq. (9), we calculate the stirring rates by summing up the contribution from all the orbits except for those collision orbits with $\tilde{r}_{\rm min} \leq 0.005$. The above choice of $\tilde{r}_{\rm min} = 0.005$ may result in underestimate of the contribution of gravitational encounters to the stirring rates compared with analytic studies such as Tanaka and Ida (1996), where direct collisions are not taken into account. However, we confirmed by orbital integrations that the results are hardly affected even if we choose smaller $\tilde{r}_{\rm min}$ ($\sim 10^{-4}$–10^{-3}), unless the random velocity is as large as the escape velocity. (Note that the mutual escape velocity $v_e = [2G(m_1 + m_2)/(R_{p1} + R_{p2})]^{1/2}$ in the current units is given as $\tilde{v}_e = v_e/R_H\Omega = ((6/\tilde{r}_p)^{1/2} \simeq 35)$. As for the range of $\tilde{b}$ for the orbital integrations, we set an upper limit as $\tilde{b}_{\rm max} = \max\{\tilde{e} + 5, 8\}$. The closest approach distance for those orbits with $\tilde{b} > \tilde{b}_{\rm max}$ is much larger than $G(m_1 + m_2)/v_{\rm rel}^2$ ($v_{\rm rel}$ is the relative velocity between planetesimals), and the viscous stirring rates due to these orbits are calculated analytically following Ida [1990, his Eq. (4.4); see also Weidenschilling (1989) and Hasegawa and Nakazawa (1990)] and added to the numerical results of orbital integrations. The contribution of these orbits with $\tilde{b} > \tilde{b}_{\rm max}$ to the dynamical friction rates can be neglected, as shown by Ida (1990).

Figure 1 shows the plots of the viscous stirring rate of eccentricity (a and b) and inclination (c and d), as a function of relative eccentricity (a and c) and inclination (b and d). In these plots, thick lines show the numerical results of orbital integration and thin lines show the analytic results obtained by Tanaka and Ida

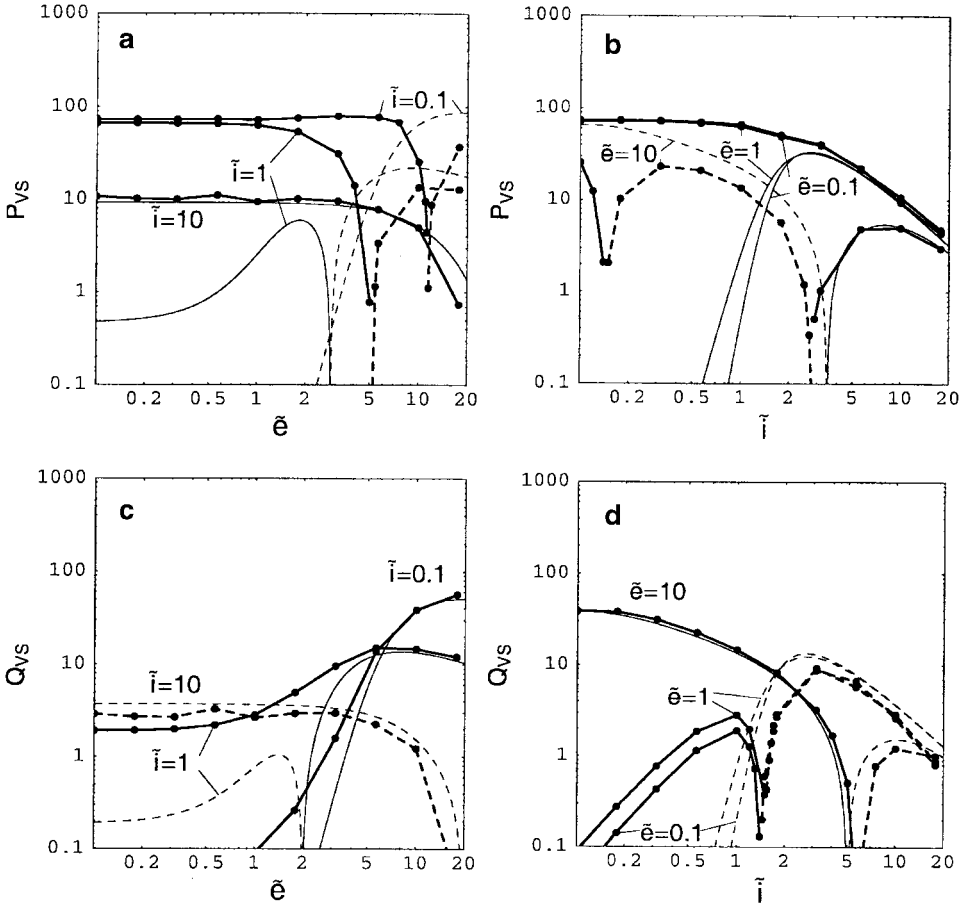

FIG. 1. Viscous stirring rates obtained by three-body orbital integrations (thick lines) and the analytic results by Tanaka and Ida (1996; thin lines). The solid lines represent positive values, while the absolute values are shown by the dashed lines when the rates take on negative values. The $\tilde{e}$-dependence for three values of $\tilde{i}$ are shown in a and c, while the $\tilde{i}$-dependence for three values of $\tilde{e}$ are shown in b and d. The solid circles on the thick lines represent the values of $\tilde{e}$ or $\tilde{i}$ for which orbital integrations were performed.

(1996, hereafter TI96), which are given as

$$P_{VS} = \frac{36}{\pi\tilde{i}\sqrt{\tilde{e}^2+\tilde{i}^2}}\left[5K(k) - \frac{12\tilde{e}^2}{\tilde{e}^2+4\tilde{i}^2}E(k)\right] \times \left[\ln(\Lambda^2+1) - \frac{\Lambda^2}{\Lambda^2+1}\right],$$
$$Q_{VS} = \frac{36}{\pi\tilde{i}\sqrt{\tilde{e}^2+\tilde{i}^2}}\left[K(k) - \frac{12\tilde{i}^2}{\tilde{e}^2+4\tilde{i}^2}E(k)\right] \times \left[\ln(\Lambda^2+1) - \frac{\Lambda^2}{\Lambda^2+1}\right], \quad (16)$$

where $K(k)$ and $E(k)$ are the complete elliptic integral of the first and second kind with $k = [3\tilde{e}^2/4(\tilde{e}^2+\tilde{i}^2)]^{1/2}$, and $\Lambda = \tilde{i}(\tilde{e}^2+\tilde{i}^2)/3$. The solid lines denote positive values, while absolute values are shown by the dashed lines when the rates take on negative values. In the relatively high-velocity cases in the dispersion-dominated region (i.e., $(\tilde{e}^2+\tilde{i}^2)^{1/2} \gtrsim 2$), gravitational encounters tend to approximately equalize orbital eccentricities and inclinations (Ida 1990). Therefore, in such high-velocity cases, P_{VS} takes on negative values when $\tilde{e} \gg \tilde{i}$, while Q_{VS} takes on negative values when $\tilde{i} \gg \tilde{e}$. We find that the numerical results agree well with the analytic ones when $\tilde{e} \gtrsim 5$, as confirmed by TI96. In such cases with high random velocities, close encounters occur in narrow restricted ranges of phase spaces, thus it becomes difficult to evaluate these rates numerically with sufficient accuracy (Ida 1990). This may have caused the discrepancy between the numerical and the analytic results in Fig. 1a for $\tilde{e} > 10$. On the other hand, in the limit of such low velocities that $\tilde{e} \ll 1$, P_{VS} and Q_{VS} tend to show constant values (Figs. 1a, 1b, and 1c), except for Q_{VS} in low $\tilde{e}$ case (Fig. 1d), where we find Q_{VS} varies as $\tilde{i}^2$.

Figure 2 shows the dependence of the dynamical friction rates on $\tilde{e}$ and $\tilde{i}$. In this case, analytic expressions are given as (TI96)

$$P_{DF} = \frac{288\tilde{e}^2}{\pi\tilde{i}(\tilde{e}^2+4\tilde{i}^2)\sqrt{\tilde{e}^2+\tilde{i}^2}}E(k)\ln(\Lambda^2+1),$$
$$Q_{DF} = \frac{288\tilde{i}^2}{\pi\tilde{i}(\tilde{e}^2+4\tilde{i}^2)\sqrt{\tilde{e}+\tilde{i}^2}}E(k)\ln(\Lambda^2+1). \quad (17)$$

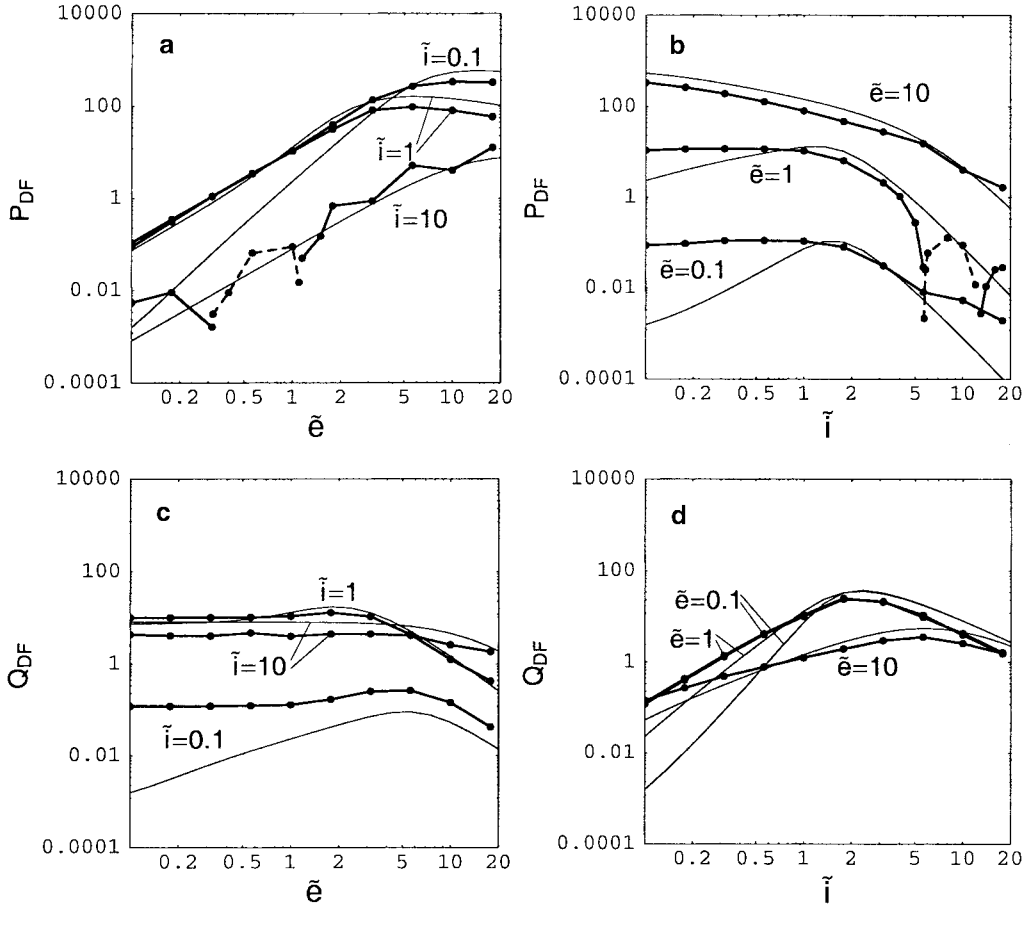

FIG. 2. Same as Fig. 1, but for dynamical friction rates.

(Note that we adopt O99's definition of P_{DF}, and Q_{DF}, which differs from that of TI96 by a factor of $\tilde{e}^2$ and $\tilde{i}^2$, respectively.) In this case, the difference between the numerical and analytic results is not so large as in the case of P_{VS} and Q_{VS}, even in the shear-dominated region. In the cases with small $\tilde{e}$ and large $\tilde{i}$, P_{DF} shows somewhat irregular behavior and it takes on even negative values occasionally. Similar irregular behavior of dynamical friction rates was found in the case of planetary rings, especially when the number of orbits for orbital integrations was not sufficiently large (O99). However, in such a low-$\tilde{e}$ and high-$\tilde{i}$ regime, $|P_{DF}|(\sim 10^{-2})$ is much smaller than P_{VS} (∼5–20); thus the effect of such irregular behavior of P_{DF} on velocity evolution can be neglected. Other than the above irregular cases, the numerical and analytic results agree quite well in the dispersion-dominated region. In the low-velocity limit of $\tilde{e} \ll 1$, on the other hand, P_{DF} and Q_{DF} take on nearly constant values in Figs. 2b and 2c, while they have positive slopes in Figs. 2a and 2d.

These results of orbital integrations are consistent with those obtained by Ida (1990). The above asymptotic behavior of viscous stirring and dynamical friction rates will be used when we calculate the Rayleigh distribution averages of these rates in next section.

2.3. *Rayleigh Distribution Averages of the Stirring Rates and Comparison with N-body Simulations*

Next, we evaluate the Rayleigh distribution averages of viscous stirring and dynamical friction rates, following the procedure described by O99. As shown in Section 2.2, the numerical results of these rates (especially, the viscous stirring rates) for a given pair of $\tilde{e}$ and $\tilde{i}$ show complicated behavior when $0.1 < \tilde{e}(\tilde{i}) \lesssim 10$. Thus, in order to evaluate their Rayleigh distribution averages, we need to fully use the numerical results of orbital integrations in this velocity range. Furthermore, the numerical results in the range of $0.1 \lesssim \tilde{e}(\tilde{i}) \lesssim 10$ are not enough to obtain the averaged rates for $0.1 \lesssim \langle\tilde{e}^2\rangle^{1/2}(\langle\tilde{i}^2\rangle^{1/2}) \lesssim 10$ with sufficient accuracy, and we further need unaveraged rates, such as $P_{VS}(\tilde{e}, \tilde{i})$, in a wider range such as $10^{-3} \le \tilde{e}(\tilde{i}) \le 10^2$ (O99). Therefore, we calculate the Rayleigh distribution averages in the following manner, as done by O99. First, using orbital integrations, we evaluate the viscous stirring and dynamical friction rates for 90 pairs of $\tilde{e}$ and $\tilde{i}$ defined as $(\tilde{e}, \tilde{i}) = (10^{(m-5)/4}, 10^{(n-5)/4})$, where $m = 1, 2, \ldots, 9$ and $n = 1, 2, \ldots, 10$, for which we were able to obtain the rates with sufficient accuracy (Section 2.2). Next, we extrapolate the numerical results to the range of $10^{-3} \le \tilde{e}(\tilde{i}) \le 10^2$, using the asymptotic behavior found in Section 2.2 as well as the analytic results (TI96). We thus obtain the stirring rates at 441 points (including the above 90 points) defined as $(\tilde{e}, \tilde{i}) = (10^{(m-13)/4}, 10^{(n-13)/4})$ $(m, n = 1, 2, \ldots, 21)$. Using these data, we perform the integral given as Eqs. (8) and evaluate the averaged rates.

SI00 analytically obtained the Rayleigh distribution averages of the stirring rates assuming that Λ in Eqs. (16) and (17) is given by

$$\Lambda = \frac{1}{3}(\langle\tilde{e}^2\rangle + \langle\tilde{i}^2\rangle)\left(\langle\tilde{i}^2\rangle^{1/2} + 1\right). \tag{18}$$

In this case, the averaged rates are obtained as

$$\begin{aligned}
\langle P_{VS}\rangle &= \langle P_{VS}\rangle'\left[\ln(\Lambda^2+1) - \frac{\Lambda^2}{\Lambda^2+1}\right],\\
\langle Q_{VS}\rangle &= \langle Q_{VS}\rangle'\left[\ln(\Lambda^2+1) - \frac{\Lambda^2}{\Lambda^2+1}\right],\\
\langle P_{DF}\rangle &= \langle P_{DF}\rangle'\ln(\Lambda^2+1),\\
\langle Q_{DF}\rangle &= \langle Q_{DF}\rangle'\ln(\Lambda^2+1),
\end{aligned} \tag{19}$$

where $\langle P_{VS}\rangle'$, etc., do not contain Λ and are given as

$$\begin{aligned}
\langle P_{VS}\rangle' &= \frac{72 I_{PVS}(\beta)}{\pi\langle\tilde{e}^2\rangle^{1/2}\langle\tilde{i}^2\rangle^{1/2}}, \quad \langle Q_{VS}\rangle' = \frac{72 I_{QVS}(\beta)}{\pi\langle\tilde{e}^2\rangle^{1/2}\langle\tilde{i}^2\rangle^{1/2}},\\
\langle P_{DF}\rangle' &= \frac{576 I_{PDF}(\beta)}{\pi\langle\tilde{e}^2\rangle^{1/2}\langle\tilde{i}^2\rangle^{1/2}}, \quad \langle Q_{DF}\rangle' = \frac{576 I_{QDF}(\beta)}{\pi\langle\tilde{e}^2\rangle^{1/2}\langle\tilde{i}^2\rangle^{1/2}},
\end{aligned} \tag{20}$$

with

$$\begin{aligned}
I_{PVS}(\beta) &= \int_0^1 \frac{5K_\lambda - \frac{12(1-\lambda^2)}{1+3\lambda^2}E_\lambda}{\beta + (\beta^{-1}-\beta)\lambda^2}\, d\lambda,\\
I_{QVS}(\beta) &= \int_0^1 \frac{K_\lambda - \frac{12\lambda^2}{1+3\lambda^2}E_\lambda}{\beta + (\beta^{-1}-\beta)\lambda^2}\, d\lambda,\\
I_{PDF}(\beta) &= \int_0^1 \frac{\frac{1-\lambda^2}{1+3\lambda^2}E_\lambda}{\beta + (\beta^{-1}-\beta)\lambda^2}\, d\lambda,\\
I_{QDF}(\beta) &= \int_0^1 \frac{\frac{\lambda^2}{1+3\lambda^2}E_\lambda}{\beta + (\beta^{-1}-\beta)\lambda^2}\, d\lambda,
\end{aligned} \tag{21}$$

where $\beta = \langle\tilde{i}^2\rangle^{1/2}/\langle\tilde{e}^2\rangle^{1/2}$, $K_\lambda = K([3(1-\lambda^2)]^{1/2}/2)$, and $E_\lambda = E([3(1-\lambda^2)]^{1/2}/2)$. SI00 also obtained the analytic expression for the contribution of distant encounters (i.e., interactions between planetesimals on noncrossing orbits) to the viscous stirring rate of eccentricity and added it to the above $\langle P_{VS}\rangle$ so that it reduces to the stirring rate obtained by three-body orbital integrations (Ida 1990) for $\langle\tilde{e}^2\rangle^{1/2}, \langle\tilde{i}^2\rangle^{1/2} \ll 1$.

Figure 3 shows the plots of viscous stirring and dynamical friction rates averaged over a Rayleigh distribution of $\tilde{e}$ and $\tilde{i}$. The thick lines show the averaged rates based on the numerical results of orbital integrations, and those calculated by SI00's analytic formulas are also shown by the thin lines for comparison. As in Figs. 1 and 2, solid lines show positive values, while dashed lines in Fig. 3a represent negative values. We show the results for three values of β; it is known that $\beta \simeq 0.5$ for relatively high random velocities, while β takes on much smaller values for low-velocity cases because $P_{VS} \gg Q_{VS}$ in such a regime (Ida 1990, Ida and Makino 1992; see also Fig. 1). It is found that

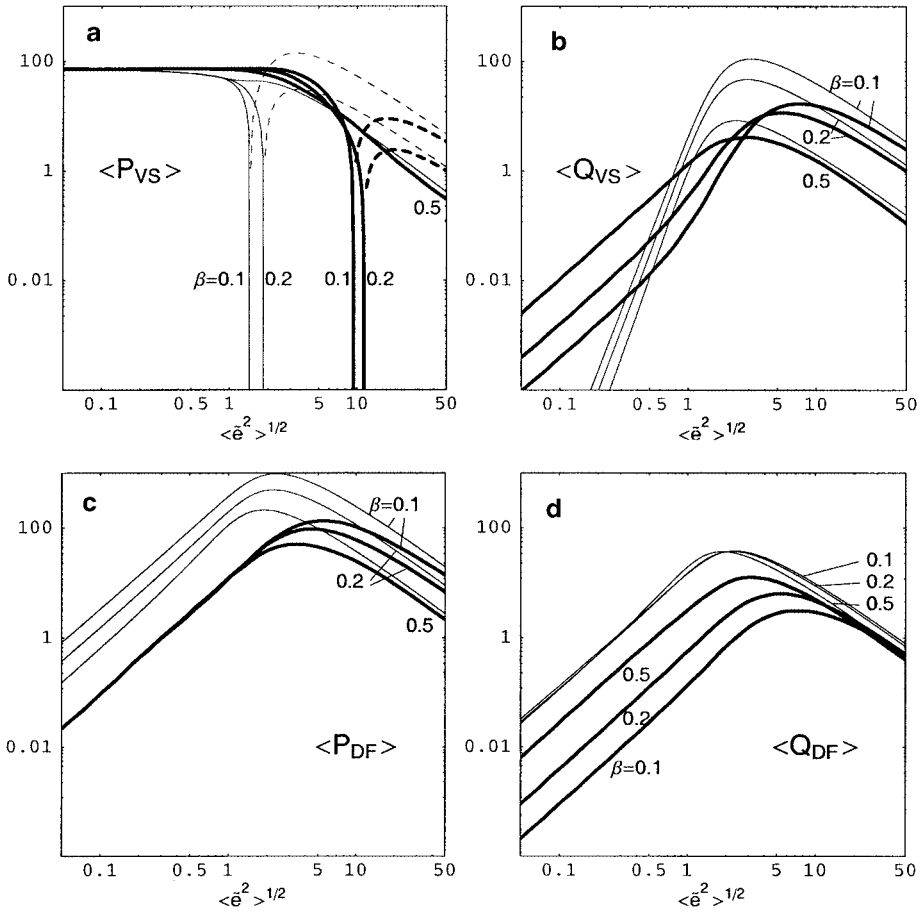

FIG. 3. Rayleigh distribution averages of viscous stirring and dynamical friction rates based on the numerical results of three-body orbital integrations (thick lines) for three different values of $\beta = \langle \tilde{i}^2 \rangle^{1/2} / \langle \tilde{e}^2 \rangle^{1/2}$. The values calculated by the analytic formulas of Stewart and Ida (2000) are also shown by the thin lines for comparison. The dashed lines in (a) represent the negative values of $\langle P_{VS} \rangle$.

SI00's analytic formulas agree well with the numerical results based on orbital integrations in the case of high velocities (i.e., $\langle \tilde{e}^2 \rangle^{1/2} \gtrsim 10$), while the deviation in $\langle Q_{VS} \rangle$, $\langle P_{DF} \rangle$, and $\langle Q_{DF} \rangle$ is significant in the shear-dominated region. In the case of $\langle P_{VS} \rangle$, the numerical and anlaytic results agree in the very low velocities ($\langle \tilde{e}^2 \rangle^{1/2} \lesssim 0.1$), since the contribution of distant encounters is added in SI00's analytic expression of $\langle P_{VS} \rangle$ so that it agrees with the three-body results in such low-velocity cases, as mentioned above. However, even in this case, notable deviation exists when $0.5 \lesssim \langle \tilde{e}^2 \rangle^{1/2} \lesssim 5$. We will discuss the comparison with SI00's results in more detail in next section.

In the low-velocity limit where $\langle \tilde{e}^2 \rangle^{1/2} \ll 1$, we find that the averaged rates based on orbital integrations can be well approximated by

$$\begin{aligned} &\langle P_{VS} \rangle_{\rm low} = 73, \quad \langle Q_{VS} \rangle_{\rm low} = 4\langle \tilde{i}^2 \rangle + 0.2 \langle \tilde{e}^2 \rangle^{3/2} \langle \tilde{i}^2 \rangle^{1/2}, \\ &\langle P_{DF} \rangle_{\rm low} = 10 \langle \tilde{e}^2 \rangle, \quad \langle Q_{DF} \rangle_{\rm low} = 10 \langle \tilde{i}^2 \rangle. \end{aligned} \tag{22}$$

For example, in the case of $0.05 \le \langle \tilde{e}^2 \rangle^{1/2} \le 0.1$ and $0.1 \le \beta \le 0.5$, we have confirmed that $\langle P_{VS} \rangle$ and $\langle Q_{VS} \rangle$ based on our orbital integrations can be approximated by Eqs. (22) within 1 and 7%, respectively, and $\langle P_{DF} \rangle$ and $\langle Q_{DF} \rangle$ agree with the above expressions within 15%. In the expression for $\langle Q_{VS} \rangle_{\rm low}$ the first term becomes dominant when $\langle \tilde{e}^2 \rangle^{1/2} \ll 1$, but the addition of the second term improves the agreement with the three-body results at $0.5 \lesssim \langle \tilde{e}^2 \rangle^{1/2} \lesssim 2$. We will use Eqs. (22) when deriving semi-analytic formulas in Section 3.

Next, we calculate velocity evolution of planetesimals using the averaged rates based on orbital integrations, and compare with N-body simulations. Although we only show the averaged rates for three cases of β in Fig. 3, those for an arbitrary pair of $\langle \tilde{e}^2 \rangle^{1/2}$ and $\langle \tilde{i}^2 \rangle^{1/2}$ can be easily calculated using the 441 data described above. Here, we calculate the evolution of root mean square eccentricities and inclinations for one- and two-component systems by solving Eqs. (6). For example, in order to simulate the evolution of root mean square eccentricities for a given surface number density and mass of planetesimals, the right-hand side of Eqs. (6) is calculated for each time step, where $\langle P_{VS} \rangle$ and $\langle P_{DF} \rangle$ are calculated by Eqs. (8) using the 441 data and the current value of $\langle \tilde{e}^2 \rangle^{1/2}$ and $\langle \tilde{i}^2 \rangle^{1/2}$. On the other hand, we also perform direct N-body simulations using the same

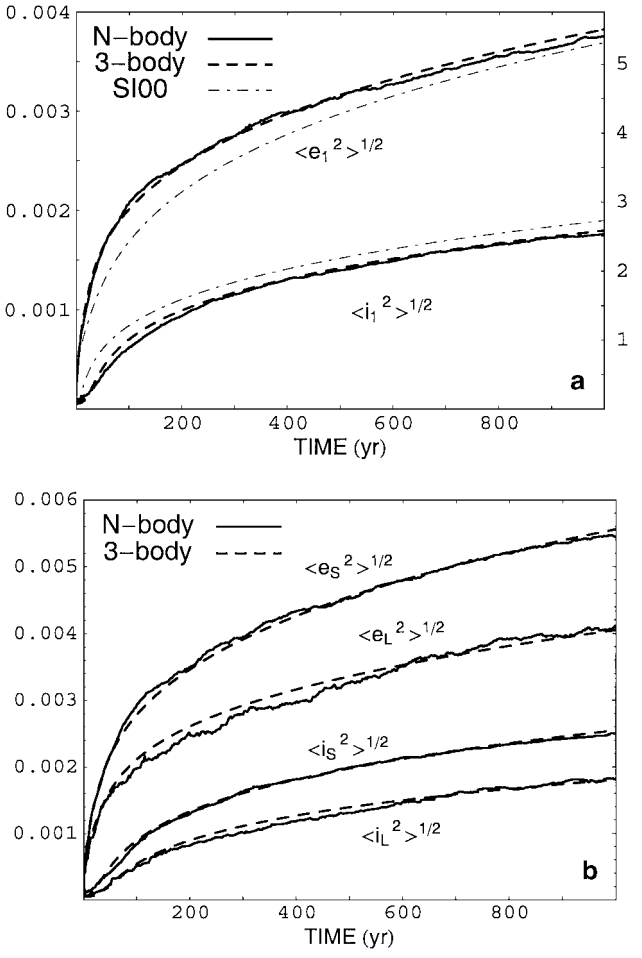

FIG. 4. Comparison of the velocity evolution calculated by Eqs. (6) and the three-body viscous stirring and dynamical friction rates (dashed lines) with the results of N-body simulations (solid lines). The integration scheme used for the N-body simulations is a fourth-order Hermite method and we used the special-purpose hardware, GRAPE-4 (Makino *et al.* 1997). (a) One component case: 1000 equal-mass ($m = 1 \times 10^{24}$ g) planetesimals are initially distributed at 1 AU with the surface density of 10 g cm^{-2} and initial r.m.s. eccentricity and inclination are 1×10^{-4} and 5×10^{-5}, respectively. The results obtained by the formulas of Stewart and Ida (2000) are also shown for comparison (thin dot–dash line). The values of r.m.s. eccentricity and inclination scaled by h_{11} (Eq. (1)) are also shown on the right ordinate. (b) Two-component case: 800 smaller planetesimals ($m = 1 \times 10^{24}$ g) and 200 larger planetesimals ($m = 4 \times 10^{24}$ g) are initially distributed at 1 AU with the total surface density of 10 g cm^{-2} and initial r.m.s. eccentricity and inclination are 1×10^{-4} and 5×10^{-5}, respectively. L and S stand for the values for the larger and smaller size component, respectively.

initial conditions for the surface number density, mass, $\langle \tilde{e}^2 \rangle^{1/2}$, and $\langle \tilde{i}^2 \rangle^{1/2}$.

Figure 4 shows the results of the comparison; solid lines represent the results of N-body simulations, while the dashed lines are obtained by solving Eqs. (6) with the three-body stirring rates. We also plot in Fig. 4a the results obtained by SI00's formulas for comparison (thin dot-dashed line). The values of $\langle e^2 \rangle^{1/2}$ and $\langle i^2 \rangle^{1/2}$ that are not scaled by the Hill radius are plotted, and we also show the values scaled by h_{11} on the right ordinate of Fig. 4a. In Fig. 4a, the evolution of root mean square eccentricity and inclination of a single size component system is shown. We find excellent agreement between the three-body results and N-body simulations; we confirm the remarkable agreement between the two results not only in the relatively high velocities in the dispersion-dominated region but also in the low velocities where Kepler shear dominates the relative velocity and the three-body effects are important. On the other hand, the results obtained by SI00's formulas deviate from the above two results in such a low-velocity regime, although the rate of evolution in the dispersion-dominated region seems consistent with the other two results (SI00). Figure 4b shows the case of two-component system, where we again find excellent agreement. These results show that velocity evolution of planetesimals with a one- or two-component system with uniform surface density can be calculated correctly using Eqs. (6) with the averaged viscous stirring and dynamical friction rates based on three-body orbital integrations, and also suggest that the velocity evolution for an arbitrary size distribution can be calculated using Eqs. (13).

2.4. Comparison with Stewart and Ida (2000) and Wetherill and Stewart (1993)

In this section, we compare our stirring rates based on orbital integrations with SI00's formulas and those reported in WS93. The comparison with these works will be further discussed in Section 4, where we calculate equilibrium velocities of planetesimals with given size distributions.

As we have seen in Fig. 3, the viscous stirring and dynamical friction rates calculated by SI00's analytic formulas agree fairly well with the three-body results when $\langle \tilde{e}^2 \rangle^{1/2} \gtrsim 10$. This is consistent with the results of SI00's comparison with N-body simulations, where they found fairly good agreement, especially in the case of a single-size component system, when random velocities are relatively high. The agreement of SI00's formulas with the three-body rates in the above high-velocity case is also consistent with the results of Inaba *et al.* (2001), who simulated accretional evolution of mass and velocity distribution by solving the coagulation equation with SI00's formulas, and found agreement with N-body simulations of planetesimal accretion. In the models simulated by Inaba *et al.* (2001) for the comparison with N-body simulations, they assumed relatively large initial mass of planetesimals ($\gtrsim 10^{23}$ g) and neglected collisional fragmentation in order to facilitate the comparison. As a result, the relative eccentricities or inclinations scaled by the Hill radius were always much larger than unity except for those between large bodies, thus the use of SI00's formulas in their simulations seems appropriate.

The disagreement in the shear-dominated regions reported in SI00 (see also Fig. 4a) can be also explained by using Fig. 3. In the case of single-component and low random velocities, SI00's simple interpolation formulas substantially underestimated the growth rate of eccentricity, while slightly overestimated that of inclination. According to their Fig. 8, the deviation in the evolution of $\langle \tilde{e}^2 \rangle^{1/2}$ and $\langle \tilde{i}^2 \rangle^{1/2}$ becomes significant when

$1 \lesssim \langle \tilde{e}^2 \rangle^{1/2} \lesssim 3$ and $\beta \sim 0.1$–0.3 (see also Fig. 4a). We confirm in Figs. 3a and 3b that SI00's formulas underestimate $\langle P_{VS} \rangle$ and overestimate $\langle Q_{VS} \rangle$ in the above velocity regime, which explains the disagreement. On the other hand, in the case of two-component system, the dynamical friction terms in SI00's formulas had to be reduced artificially by 30% to obtain better agreement with N-body simulations. This is explained in Figs. 3c and 3d, which show that their analytic formulas for dynamical friction rates substantially overestimate the three-body results when $\langle \tilde{e}^2 \rangle^{1/2} \lesssim 10$.

It should be noted that TI96's analytic results for the unaveraged dynamical friction rates (Eq. (17)), if the factors of $\tilde{e}^2$ and $\tilde{i}^2$ are corrected as mentioned in Section 2.2, reproduce well the three-body results down to $\tilde{e} \simeq 2$ (Fig. 2), while SI00's analytic results for the Rayleigh distribution averages of these rates show good agreement only when $\langle \tilde{e}^2 \rangle^{1/2} \gtrsim 10$. This comes from the fact that SI00 adopted the approximate expression for Λ given by Eq. (18) when evaluating the Rayleigh distribution averages. In order to demonstrate this, we have numerically evaluated the Rayleigh distribution average of P_{DF} using Eq. (17) and compare with the three-body results in Fig. 5. We find that agreement between the two results is much improved in the above intermediate velocity regime, if the Rayleigh distribution average is correctly calculated (compare with Fig. 3c).

Next, we compare our results with WS93's expressions. WS93 used their analytic expressions to evaluate the stirring rates in the dispersion-dominated regime, and used the values of the analytic results for the high-velocity cases and the velocity-dependence of the numerical results of Ida's (1990) orbital integrations to obtain the stirring rates in the shear-dominated regime. Now the work of SI00 allows us to directly compare WS93's expressions for velocity stirring rates with the formulas based on the Hill formalism (Ida 1990, O99), including ours. In this case, it should be noted that WS93's definition of the viscous stirring and dynamical friction terms slightly differs from those used in the Hill formalism. In our definition given by Eqs. (6), the viscous stirring term is proportional to m_j^2, while in WS93's definition, it is proportional to $m_j(m_1 + m_j)$ and their dynamical friction rate corresponds to the sum of $\langle P_{VS} \rangle + \langle P_{DF} \rangle$ (or $\langle Q_{VS} \rangle + \langle Q_{DF} \rangle$) in our definition (see also SI00). SI00 discussed a comparison between their analytic formulas and WS93's expressions in high-velocity cases. As stated in SI00, SI00's formulas reduce to the expressions similar to WS93's if the approximation of $\Lambda \gg 1$ is applied, but the rates of viscous stirring and dynamical friction of inclinations as well as the rate of dynamical friction of eccentricities reported in WS93 were a factor of 2 or 4 overestimated compared to the results of SI00. Owing to these errors in the coefficients and the different definition of the terms, WS93's expressions cannot be rewritten into forms directly comparable to our $\langle P_{VS} \rangle$, etc. However, we can evaluate the viscous stirring and dynamical friction terms defined by WS93 using our $\langle P_{VS} \rangle$, etc., to compare with WS93's results, as done by SI00. Other than the disagreement caused by the errors in the coefficients, we also found the following features of WS93's stirring rates in the shear-dominated cases from this comparison: (i) The velocity-dependence of WS93's viscous stirring and dynamical friction rates for inclinations in the shear-dominated region ($\propto \langle \tilde{i}^2 \rangle$) agrees with the three-body results as expected, but the absolute values are over-estimated by a factor of 5–10 for $\beta = 0.5$ and more than 10^2 for $\beta = 0.1$, because of their simplified method of extrapolation. (ii) WS93 assumed that their dynamical friction rate of eccentricities in the shear-dominated region is proportional to $\langle \tilde{e}^2 \rangle$, on the basis of Ida's (1990) numerical results. However, as mentioned above, their dynamical friction rate corresponds to $\langle P_{VS} \rangle + \langle P_{DF} \rangle$ in our notations, and this quantity is dominated by $\langle P_{VS} \rangle$ in such low-velocity cases, where $\langle P_{VS} \rangle$ takes on constant values (Fig. 3a). As a result, WS93's expression for dynamical friction rate of eccentricities underestimates the three-body results when $\langle \tilde{e}^2 \rangle^{1/2} \lesssim 1$. (iii) WS93's expression for the viscous stirring rate of eccentricities in the shear-dominated region gives a constant value, as in the case of the three-body results, but the absolute value is underestimated by a factor of about 2 compared to the three-body results, owing to their simplified method of extrapolation.

In next section, we will derive new semi-analytic formulas which reproduce well the numerical results of three-body orbital integrations in both shear- and dispersion-dominated velocity regions, by combining the expressions for low velocities (Eq. (22)) and those similar to SI00's formulas for high-velocity (close) encounters but with revised expression for Λ.

3. SEMI-ANALYTIC FORMULAS FOR THE STIRRING RATES

First, we derive analytic formulas for high velocities, by slightly changing the SI00's expressions. We assume that the Rayleigh distribution averages of Eqs. (16) and (17) can be approximated by the expressions,

$$\begin{aligned} \langle P_{VS} \rangle_{\rm high} &= \langle P_{VS} \rangle' \ln(\Lambda^2 + 1), \\ \langle Q_{VS} \rangle_{\rm high} &= \langle Q_{VS} \rangle' \ln(\Lambda^2 + 1), \\ \langle P_{DF} \rangle_{\rm high} &= \langle P_{DF} \rangle' \ln(\Lambda^2 + 1), \\ \langle Q_{DF} \rangle_{\rm high} &= \langle Q_{DF} \rangle' \ln(\Lambda^2 + 1), \end{aligned} \tag{23}$$

where $\langle P_{VS} \rangle'$, etc., are given by Eqs. (20). The above expressions for $\langle P_{DF} \rangle_{\rm high}$ and $\langle Q_{DF} \rangle_{\rm high}$ are the same as those given by Eqs. (19), except the expression for Λ, which will be given below. Note that we neglected $\Lambda^2/(\Lambda^2 + 1)$ in the expressions of $\langle P_{VS} \rangle_{\rm high}$ and $\langle Q_{VS} \rangle_{\rm high}$, because we practically use Eqs. (23) only for high-velocity cases where $\Lambda^2/(\Lambda^2 + 1) \ll \ln(\Lambda^2 + 1)$ and replace them with Eqs. (22) for low-velocity cases (see (25) below), and also because it is not clear if the Λ-dependence of the averaged stirring rates should be exactly the same as that of Eqs. (16).

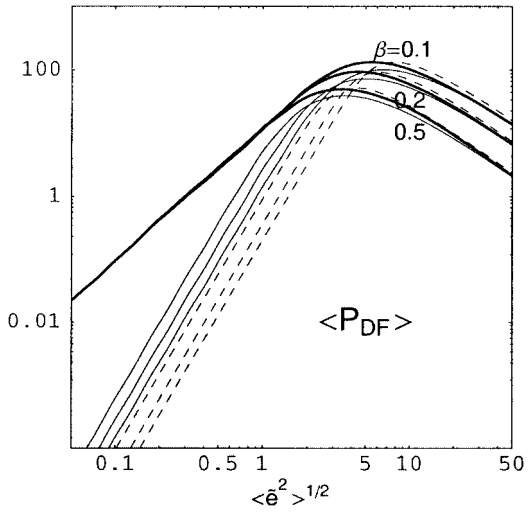

FIG. 5. Comparison of $\langle P_{DF}\rangle$ based on the three-body orbital integrations (thick lines) and those obtained by numerical integration of Eq. (8) with the analytic result (Eq. (17)) of Tanaka and Ida (1996) (thin solid lines). The dashed lines represent the analytic results for high-velocity cases (Eq. (23)) with revised expression for Λ given by Eq. (24) (see Section 3).

Since $\langle P_{VS}\rangle'$, etc., are already obtained by SI00, we tried to find an appropriate expression for Λ in Eqs. (23) by comparing $\langle P_{VS}\rangle_{\rm high}$, etc., with the three-body results in the high-velocity cases ($\langle\tilde{e}^2\rangle^{1/2} \gtrsim 5$) with various values of β. We find that the three-body results in the above velocity regime can be reproduced quite well when Λ is given by

$$\Lambda = \frac{1}{12}(\langle\tilde{e}^2\rangle + \langle\tilde{i}^2\rangle)\langle\tilde{i}^2\rangle^{1/2}. \tag{24}$$

As an example, $\langle P_{DF}\rangle_{\rm high}$ calculated with the above Λ is plotted with the dashed lines in Fig. 5, where we find much improved agreement in the high velocities ($5 \lesssim \langle\tilde{e}^2\rangle^{1/2} \lesssim 20$) compared to Fig. 3c. In the case of $\langle\tilde{i}^2\rangle^{1/2} \gg 1$, the above Λ is four times smaller than the expression adopted by SI00 (Eq. (18)), who substituted $\langle\tilde{e}^2\rangle^{1/2}$ and $\langle\tilde{i}^2\rangle^{1/2}$ for $\tilde{e}$ and $\tilde{i}$ in the original form of $\Lambda = \tilde{i}(\tilde{e}^2 + \tilde{i}^2)/3$ in Eqs. (16) and (17) for the nonaveraged stirring rates. This reflects the fact that the stirring rates are decreasing functions of $\tilde{e}$ and $\tilde{i}$ in the high-velocity regime (Eqs. (16) and (17)) and low-velocity particles are more abundant in the case of the Rayleigh distribution so that they are the major contributor to the averaged stirring rates. As a result, rather than substituting $\langle\tilde{e}^2\rangle^{1/2}$ and $\langle\tilde{i}^2\rangle^{1/2}$ for $\tilde{e}$ and $\tilde{i}$ in the original form of Λ in Eqs. (16) and (17), substitution of slightly smaller values can approximate better the exact average values of the stirring rates. The reduction factor of 4 is determined empirically by the comparison with the three-body results.

Next, we combine Eqs. (22) and (23) to obtain new semi-analytic formulas, which are valid for both low- and high-velocity cases. We obtained the following formulas that can reproduce the three-body results quite well;

$$\begin{aligned}
\langle P_{VS}\rangle &= C_1\langle P_{VS}\rangle_{\rm low} + \langle P_{VS}\rangle_{\rm high},\\
\langle Q_{VS}\rangle &= C_2\langle Q_{VS}\rangle_{\rm low} + \langle Q_{VS}\rangle_{\rm high},\\
\langle P_{DF}\rangle &= C_3\langle P_{DF}\rangle_{\rm low} + \langle P_{DF}\rangle_{\rm high},\\
\langle Q_{DF}\rangle &= C_3\langle Q_{DF}\rangle_{\rm low} + \langle Q_{DF}\rangle_{\rm high},
\end{aligned} \tag{25}$$

where

$$\begin{aligned}
C_1 &= \ln(10\Lambda^2/\langle\tilde{e}^2\rangle + 1)/(10\Lambda^2/\langle\tilde{e}^2\rangle),\\
C_2 &= \ln\bigl(10\Lambda^2\langle\tilde{e}^2\rangle^{1/2} + 1\bigr)\big/\bigl(10\Lambda^2\langle\tilde{e}^2\rangle^{1/2}\bigr),\\
C_3 &= \ln(10\Lambda^2 + 1)/10\Lambda^2,
\end{aligned} \tag{26}$$

and Λ is given by Eq. (24). The functional form and the coefficient of 10 in the expressions of C_1 to C_3 are determined empirically by the comparison with the three-body results, and the difference in the $\langle\tilde{e}^2\rangle$-dependence of C_1 to C_3 reflects the different dependence of the stirring rates on $\langle\tilde{e}^2\rangle$ or $\langle\tilde{i}^2\rangle$ in the low-velocity limit (Eqs. (22)). Note that $\langle P_{VS}\rangle$, etc., reduce to $\langle P_{VS}\rangle_{\rm low}$, etc., and $\langle P_{VS}\rangle_{\rm high}$, etc., in the low- ($\Lambda \ll 1$) and high- ($\Lambda \gg 1$) velocity limit, respectively.

Figure 6 compares the above semi-analytic formulas (thin lines) with the three-body results (thick lines), where we find fairly good agreement for the entire velocity regions. Recall that $\beta \simeq 0.5$ for high-velocity cases, while β takes on much smaller values for low-velocity cases (Ida and Makino 1992). Therefore, in the low-velocity cases, analytic formulas should reproduce the three-body results with $\beta \lesssim 0.5$, while it is sufficient if they reproduce the three-body results of $\beta \simeq 0.5$ in the high-velocity cases. We find that our new formulas satisfy the above criterion quite well.

We also calculate the velocity evolution using the above formulas and compare with N-body simulations in Fig. 7. We find excellent agreement both in one- and two-component systems, and the agreement seems to be almost the same as in the case of Fig. 4, where we used the numerical results of three-body orbital integrations.

The above expressions of the semi-analytic formulas have been obtained by simply combining the two expressions for low- and high-velocity cases and comparing with the three-body results, and one may be able to obtain more complicated formulas which agree better with the three-body results. However, excessively complicated analytic formulas are not suitable for numerical simulations of planetary accretion using a coagulation equation, where it is desirable to calculate velocity evolution without wasting computing time. Moreover, the important quantity that controls the growth rate of planets is the equilibrium velocity of planetesimals, which is determined by the balance between gravitational encounters, direct collisions, and drag force by the solar nebula gas (if it exists). In this case, the dependence of the value of the equilibrium velocity on the

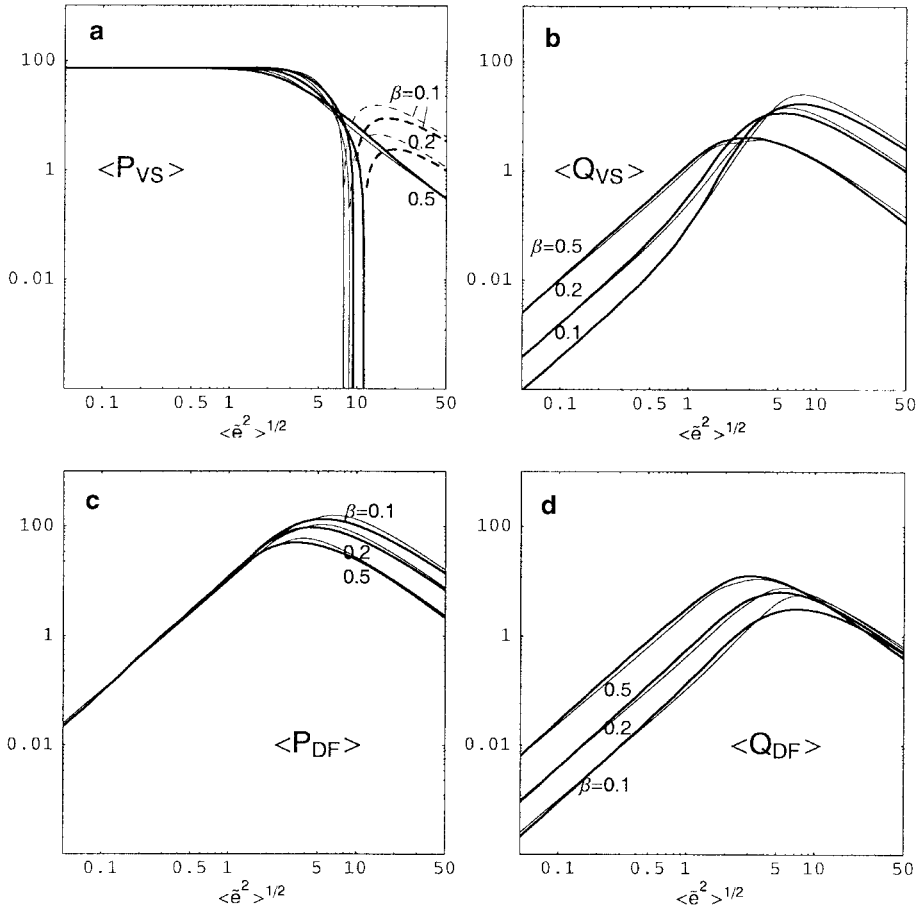

FIG. 6. Comparison of the Rayleigh distribution averages of viscous stirring and dynamical friction rates calculated by the new analytic formulas (Eqs. (25); thin lines) with those obtained by three-body orbital integrations (thick lines) for three different values of $\beta = \langle \tilde{i}^2 \rangle^{1/2} / \langle \tilde{e}^2 \rangle^{1/2}$. The dashed lines in (a) represent the negative values of $\langle P_{VS} \rangle$.

stirring rates (such as $\langle P_{VS} \rangle$) is weaker compared to the sensitive dependence of the velocity evolution rate on the stirring rates. As an example, let us consider the equilibrium velocity in a swarm of equal-sized planetesimals by the balance between gravitational encounters and gas drag. The time scale of velocity stirring due to gravitational encounters is roughly given by $T_{\rm grav} = \langle \tilde{e}^2 \rangle / (d\langle \tilde{e}^2 \rangle / dt)_{\rm grav} \propto \langle \tilde{e}^2 \rangle / \langle P_{VS} \rangle$, while that of velocity damping due to gas drag can be written as $T_{\rm gas} = \langle \tilde{e}^2 \rangle / (d\langle \tilde{e}^2 \rangle / dt)_{\rm gas} \propto \langle \tilde{e}^2 \rangle^{-1/2}$, when $\langle \tilde{e}^2 \rangle^{1/2}$ ($\simeq \langle \tilde{i}^2 \rangle^{1/2}$) is relatively large (e.g., Inaba *et al.* 2001). Equating $T_{\rm grav}$ to $T_{\rm gas}$, we find that the equilibrium eccentricity roughly satisfies a relation $\langle \tilde{e}^2 \rangle_{eq}^{1/2} \propto \langle P_{VS} \rangle^{1/3}$, which shows that the change in the equilibrium velocity is only 25% even if $\langle P_{VS} \rangle$ changes by a factor of two. As we have shown in Fig. 6, the stirring rates calculated by our new formulas agree with the three-body results with sufficient accuracy both in low- and high-velocity regimes. Therefore, slightly more accurate formulas than ours with much more complicated expressions would hardly affect the results obtained by our formulas if they are used to calculate the equilibrium velocities of planetesimals, and we think that our new formulas are sufficiently simple and accurate (as demonstrated in Fig. 7).

4. EQUILIBRIUM VELOCITIES OF PLANETESIMALS AND GROWTH RATE OF PROTOPLANETS

In order to demonstrate how our new formulas derived in Section 3 would affect planetary growth, here we calculate equilibrium velocities of planetesimals and the growth rate of the largest bodies for assumed size distributions, corresponding to three stages of accretion.

We consider an annular zone located at $a = 1$AU with $\Delta a = 0.15$AU that includes 3.2×10^{27} g of solid bodies (surface density is 15 g cm^{-2}). On the basis of the numerical results of accretional simulations by WS93, we assume a system of three components, which we will call "collisional fragments" (10^7 g $\leq m < 5 \times 10^{18}$ g with $n(m) \propto m^{-11/6}$, where $n(m)$ is the incremental size distribution function), "planetesimals" (5×10^{18} g $\leq m \leq 3 \times 10^{23}$ g with $n(m) \propto m^{-8/3}$), and "runaway bodies" (which will be taken into account only in the later two stages).

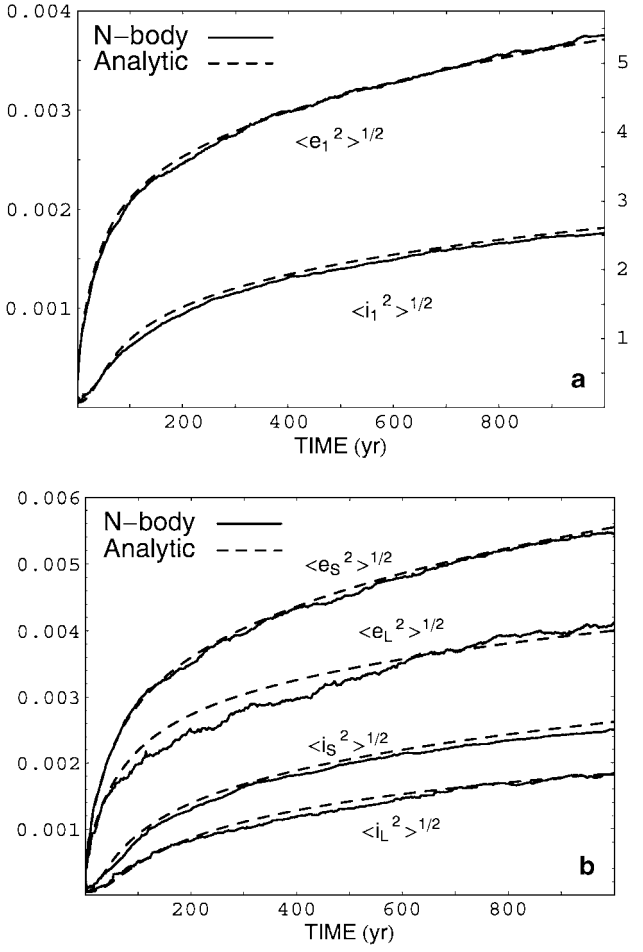

FIG. 7. Comparison of the velocity evolution calculated by Eqs. (6) and the new analytic formulas (Eqs. (25); dashed lines) with the results of N-body simulations (solid lines). (a) One component case, and (b) two component case. The initial conditions are the same as in Fig. 4.

The range of sizes of each component was chosen based on the numerical results of WS93. The above power-law size distributions of collisional fragments and planetesimals approximately reproduce the numerical results of WS93, and have been also supported by analytic studies (Tanaka *et al*. 1996, Makino *et al*. 1998). We consider the size distributions at three different stages of planetary accretion: (a) before the onset of runaway growth; (b) early stage of runaway growth, where accretion of planetesimals ($m \gtrsim 10^{18}$ g) mostly contributes to the growth of runaway bodies; and (c) later stage of runaway growth, where accretion of collisional fragments ($m < 10^{18}$ g) significantly contributes to the growth of runaway bodies. The above three stages roughly correspond to $t \simeq 7 \times 10^3$ years, 2×10^4 years, and 6×10^4 years from the start of the simulation shown in Figs. 1 to 3 of WS93 (Stages B, C, and D, in their figures), respectively. We assume that 10 runaway bodies on isolated orbits are formed at the stages (b) and (c), and their masses (2×10^{25} g and 5×10^{25} g in (b) and (c), respectively) and the numbers of bodies in the other two components are chosen so that the mass fraction of each component roughly agree with WS93's results (Fig. 8). The mass fraction of each component (fragments : planetesimals : runaway bodies) in our assumed size distribution at each stage is: (a) 0.0003 : 0.9997 : 0, (b) 0.02 : 0.92 : 0.06, and (c) 0.11 : 0.73 : 0.16.

For each of the above three assumed size distributions, we calculate equilibrium velocities (i.e., r.m.s. eccentricities and inclinations) as a function of mass. Here, in addition to gravitational encounters, we also take into account the effects of gas drag and inelastic collisions (see Appendix for the detailed description for the method of calculations). We assume that all the bodies have r.m.s. eccentricities and inclinations equal to 10^{-4} initially, and solve Eqs. (13) with the additional terms for gas drag and inelastic collisions up to $t = 5 \times 10^3$ years, when we confirm that a quasi-equilibrium velocity distribution is achieved for a given size distribution. We find that the quasi-equilibrium velocity distribution is insensitive to the choice of initial velocity distribution and is achieved in about $\sim 10^3$ years. For each size distribution, we also calculate the mass accretion rate of runaway bodies (and that of largest bodies in the case (a)), using the given size distribution and calculated velocity distribution (Appendix).

As for the calculations of velocity stirring rates due to gravitational encounters, we use three different formulas: Our new formulas derived in Section 3, SI00's formulas, and the expressions used in WS93. First, we compare our formulas with SI00's. Then, we also compare ours with WS93's.

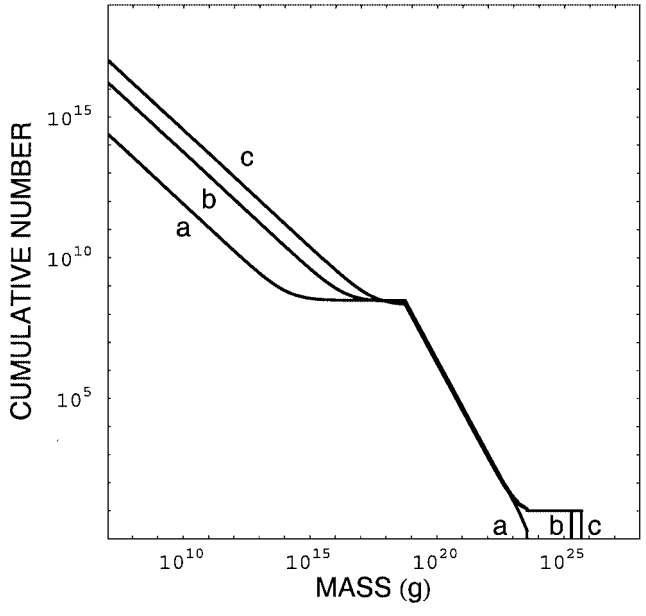

FIG. 8. Cumulative mass distributions for the three cases a, b, and c, used for the calculations of equilibrium velocity distributions.

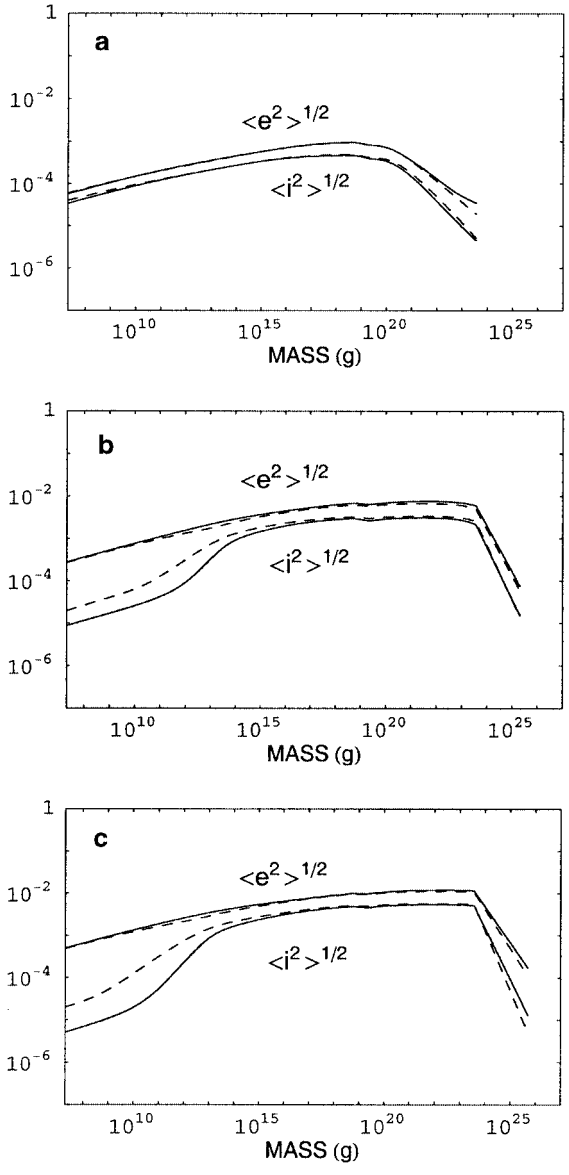

FIG. 9. Distribution of r.m.s. eccentricities and inclinations as a function of mass for the three size distributions a, b, and c, as shown in Fig. 8. The solid lines are the results obtained by using our new formulas (Eqs. (25)), and the dashed lines are produced by using the analytic formulas of Stewart and Ida (2000).

Figure 9 shows the velocity distributions obtained by these calculations. The solid lines are the results obtained by our new formulas, and the dashed lines are produced by SI00's formulas ($\langle P_{DF}\rangle$ and $\langle Q_{DF}\rangle$ given by Eqs. (19) were multiplied by 0.7 when we use SI00's formulas, following SI00).

Stage (a)

At this stage, the two results obtained by our formulas and SI00's agree very well with each other (Fig. 9a), since the relative velocities scaled by the Hill radius is relatively large ($\gtrsim$2) with $\beta \simeq 0.5$, except for those between large bodies ($m \simeq 10^{22-23}$ g). This is also consistent with the result of Inaba *et al.* (2001), who simulated planetesimal accumulation using a coagulation equation with SI00's formulas and found good agreement with N-body simulations in the case that planetesimal velocities remain relatively high. We find that both eccentricities and inclinations of planetesimals at this stage are determined mainly by the balance between the enhancement due to the viscous stirring caused by large bodies ($m \simeq 10^{22-23}$ g) and damping by gas drag. On the other hand, in the case of largest bodies ($m \sim 10^{23}$ g), their eccentricities are determined by the balance between viscous stirring by large bodies ($m \simeq 10^{22-23}$ g) and dynamical friction by small planetesimals ($m \simeq 10^{18-19}$ g), while their inclinations are determined by the enhancement (viscous stirring and energy input as a counteraction of dynamical friction) by planetesimals with $m \simeq 10^{20}$ g and damping due to the dynamical friction by small planetesimals ($m \simeq 10^{18-19}$ g). The relative inclinations between largest bodies and planetesimals with $m \simeq 10^{18-19}$ g (which are the major contributor to the growth of largest bodies) is slightly smaller in the case with our new formulas than the case with SI00's, because SI00's formulas overestimate $\langle Q_{VS}\rangle$ for $\langle \tilde{e}^2\rangle^{1/2} \simeq 2$ (Fig. 3b). As a result, the growth rate of largest bodies at this stage is about 10% larger with our new formulas compared to the case with SI00's.

Stage (b)

In Fig. 9b, we note significant deviation between the two results in the inclination distribution of fragments at this stage, while the two results for eccentricity distribution agree quite well. At this stage, the eccentricities of fragments are determined mainly by the balance between the viscous stirring by runaway bodies and damping by gas drag, and the relative eccentricities between the fragments and the runaway bodies scaled by their mutual Hill radius are ~0.1–2.0. In this case, the two results for the eccentricity distribution of fragments agree well, as $\langle P_{VS}\rangle$ in the SI00's formulas was defined so that it reproduces the three-body results in the limit of $\langle \tilde{e}^2\rangle^{1/2} \ll 1$. On the other hand, in the case of inclinations of fragments, viscous stirring by the runaway bodies becomes less effective for such low relative velocities (Fig. 3b). Instead, in the case with our new formulas, the inclinations of the fragments are mainly enhanced by the viscous stirring and energy input from large planetesimals ($m \simeq 10^{22-23}$ g) and damped by gas drag. In the case with SI00's formulas, however, we find that the inclinations of fragments are enhanced mainly by energy input from the runaway bodies. This is because SI00's formulas overestimate the values of $\langle Q_{DF}\rangle$ especially when β is small (Fig. 3d). We find in Fig. 3d that the values of $\langle Q_{DF}\rangle$ obtained by SI00's formulas are almost independent of β in low-velocity cases, so that they are larger than the three-body results by more than two orders of magnitude when

$\beta = 0.1$. As a result, the inclinations of the fragments in the case with SI00's formulas become significantly larger than the case with our new formulas. This deviation becomes significant when the relative inclinations between the fragments and the runaway bodies scaled by their mutual Hill radius become smaller than unity, where β takes on the values much smaller than 0.5. This corresponds to $m \sim 10^{15}$ g, where the two results for inclination distribution start to deviate significantly. As a result of the fragments' lower inclinations and higher collision rate, the mass accretion rate of fragments onto the runaway bodies with the new formulas is about 20% larger than that with SI00's formulas. However, as we mentioned above, the growth of runaway bodies at this stage is mainly due to accretion of planetesimals ($m \gtrsim 10^{18}$ g), rather than the fragments (WS93). Moreover, the dependence of the accretion rate on inclinations becomes weak when $\langle \tilde{e}^2 \rangle^{1/2} \ll 1$ (Ida and Nakazawa 1989, Greenzweig and Lissauer 1990, 1992). As a result, the difference in the growth rates of the runaway bodies in the two cases is about 10%, owing mainly to the slightly smaller inclinations of planetesimals with $m \simeq 10^{18-19}$ g, as in stage (a).

Stage (c)

The velocity distributions are quite similar to those at the stage (b), and we find in Fig. 9c more significant difference between the two results for the inclination distribution of the fragments (the inclinations of runaway bodies in the case with SI00's formulas become also smaller due to the strong dynamical friction by the fragments). The mass accretion rate of fragments onto the runaway bodies with the new formulas is about 30% larger than that with SI00's formulas. However, in contrast to the stage (b), this difference is now important, as accretion of fragments significantly contributes to the growth of the runaway bodies (WS93). The fraction of the total mass of the system in the form of fragments is now more than five times as large as that at the stage (b), and these fragments are accreted by the runaway bodies more easily with their lower inclinations. We find that the growth rate of the runaway bodies in the case with our new formulas is larger than the case with SI00's by about 20%.

In summary, we have confirmed that SI00's formulas describe the distributions of eccentricities and inclinations very accurately in the dispersion-dominated regime ($\langle \tilde{e}^2 \rangle^{1/2} \gtrsim 2$; Fig. 9a), and they also predict the eccentricity distribution with sufficient accuracy even in the shear-dominated region (Figs. 9b and 9c). However, SI00's formulas tend to overestimate the values of inclinations of small fragments when the relative velocities between these fragments and runaway bodies become too small to ignore the effects of the solar gravity.

Figure 10 shows the results of a similar comparison, but the dashed lines in this case are obtained by using WS93's expressions for the viscous stirring and dynamical frictions rates. The general features of Fig. 10 are similar to Fig. 9, but there are several slight differences between the dashed lines in Figs. 9 and 10, reflecting the differences between SI00's formulas and WS93's. At stage (a), the solid and dashed lines agree with each other fairly well, but both eccentricities and inclinations of small bodies calculated by WS93's formulas are slightly larger than those obtained from our formulas. This is mainly because WS93's dynamical friction rates (which corresponds to the sum of the viscous stirring rate and the dynamical friction rate in our definition, as mentioned in Section 2.4; see also SI00) for eccentricity and inclination overestimate the three-body results when $2 \lesssim \langle \tilde{e}^2 \rangle^{1/2} \lesssim 10$, owing to the errors in their coefficients (SI00) and their simplified method of extrapolation. However, this deviation is notable only for the small fragments (Fig. 10a),

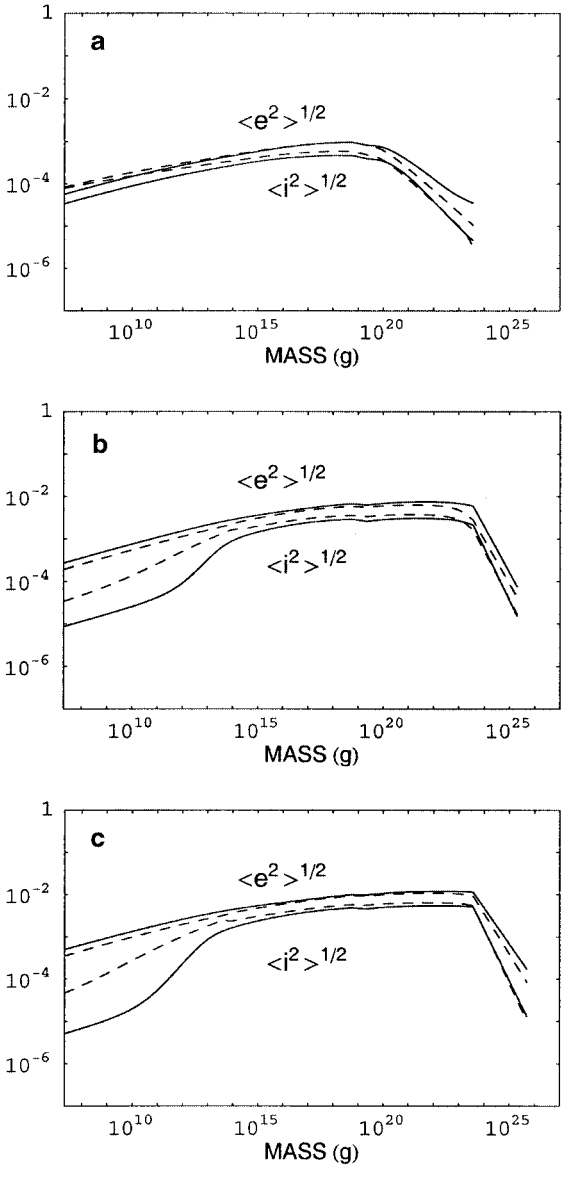

FIG. 10. Same as Fig. 9, but the dashed lines are produced by using the formulas of Wetherill and Stewart (1993).

whose contribution to the growth of the largest bodies is negligible at this stage. As a result, the growth rate of the largest bodies calculated in the case of WS93's formulas agrees with the three-body results within 6%. At stage (b), eccentricities of the fragments calculated by WS93's formulas are slightly smaller than those obtained from our formulas (Fig. 10b). This is because WS93's formulas underestimate the viscous stirring rate of eccentricity in the shear-dominated regime, owing to their simplified method of extrapolation (Section 2.4). On the other hand, inclinations of the fragments are larger than the three-body case, because WS93's formulas overestimate the dynamical friction rate of inclination in low-velocity cases with small values of β, as in the case of SI00's formulas (Fig. 3d). Since WS93's viscous stirring rate and dynamical friction rate of inclination is a factor of 2 and 4 larger than SI00's owing to the errors in the coefficients, the values of inclinations of small fragments in Fig. 10b calculated by WS93's formulas are still larger than the case with SI00's formulas (Fig. 9b). This also results in the slightly larger values of inclinations of planetesimals that mostly contribute to the growth of the runaway bodies. As a result, the growth rate of the runaway bodies at this stage in the case of WS93's formulas is about 20% smaller compared to the case with our formulas based on three-body orbital integrations. The velocity distribution at stage (c) (Fig. 10c) is similar to that at stage (b). We find that the growth rate of the runaway bodies at this stage in the case of WS93's formulas is about 30% smaller than the case with ours.

The fairly good agreement in the velocity distribution just before the onset of runaway growth among the results with the three formulas (Figs. 9a and 10a) leads us to support the previously found results such as runaway growth of protoplanets (e.g., Wetherill and Stewart 1989, 1993). However, the above comparisons also suggest that our new formulas could affect the growth rate of protoplanets, especially in the stage after early runaway growth, where small fragments can significantly contribute to the rapid growth of runaway bodies (WS93). The above results suggest that the growth rate at such a stage can be enhanced by $\sim$20–30% compared to the cases using the formulas of SI00 or WS93. However, it is desirable to carry out simulations using a coagulation equation to confirm the above results, as the above estimates are based on the simple model for the size distributions of fragments, planetesimals, and runaway bodies. Inclusion of radial migration of planetesimals (especially, inward drift and removal of small fragments due to gas drag) is also necessary for a more precise estimate of the growth rate of protoplanets (WS93, Weidenschilling *et al*. 1997).

5. CONCLUSIONS AND DISCUSSION

In the present work, we obtained the viscous stirring and dynamical friction rates of planetesimals with a Rayleigh distribution of eccentricities and inclinations, using three-body orbital integration. We found that the results agree well with the analytic formulas of Stewart and Ida (2000) in the high-velocity cases where planetesimals' random motion dominates their relative velocity. In low-velocity cases where Kepler shear dominates the relative velocity, however, the three-body calculations show significant deviation from the formulas of Stewart and Ida, who did not investigate the rates for low velocities in detail but just presented a simple interpolation formula between their high-velocity formula and the numerical results for circular orbits. We calculated the evolution of r.m.s. eccentricities and inclinations using these three-body stirring rates and confirmed excellent agreement with the results of N-body simulations. We derived new semi-analytic formulas for the viscous stirring and dynamical friction rates that can reproduce the three-body results. Therefore, the velocity evolution equations given by Eqs. (13) together with our newly obtained semi-analytic formulas (Eqs. (25) with Eqs. (22)–(24), and (26)) can be used to predict the velocity evolution of planetesimals with a wide range of sizes that cannot be simulated by direct orbital integrations.

We also calculated equilibrium velocity distributions of planetesimals for assumed size distributions. We found that the velocity distribution before the onset of runaway growth obtained by our new formulas agree well with that calculated by the analytic formulas derived by Stewart and Ida (2000), as the relative velocities between planetesimals are rather high at this stage. The expressions for the velocity stirring rates reported in Wetherill and Stewart (1993) were also found to predict the velocity distribution at this stage quite well. However, at the later stage where large bodies are formed as a results of runaway growth, the inclinations of small collisional fragments calculated by our new formulas were found to become much smaller than those obtained by Stewart and Ida's formulas or those reported in Wetherill and Stewart (1993), so that these small fragments are more easily accreted by large bodies in our case. This could enhance the growth rate of runaway bodies in the intermediate stage of accretion, where these fragments significantly contribute to the rapid growth of large bodies, and could reduce the formation time of planetary embryos in the terrestrial zone (WS93, Weidenschilling *et al*. 1997) and those in outer solar system such as Kuiper belt objects (Kenyon and Luu 1998, 1999).

In Section 4, we calculated the velocity distributions and accretion rates of runaway bodies for assumed size distributions based on the the numerical results of Wetherill and Stewart (1993). The purpose of such calculations was to clarify the expected difference in the outcome of the simulations of planetesimal accumulation with our new formulas compared to the cases with previously obtained formulas for velocity evolution. For this reason, we used a rather simple model, neglecting evolution of size distribution, radial migration of planetesimals, etc. The results of the present work can be used to produce more accurate numerical simulations of early stages of planetary accretion, in combination with the technique of calculating

the evolution of size distribution with great precision (Wetherill 1990, Weidenschilling *et al*. 1997, Inaba *et al*. 1999, 2001).

APPENDIX

We calculate the evolution of r.m.s. eccentricities and inclinations for given size distributions shown in Fig. 8, taking into account the effects of gravitational encounters, gas drag, and inelastic collisions, in the following ways. The collisional fragments and planetesimals, which have continuous size distributions as shown in Fig. 8, are divided into 56 logarithmically spaced mass bins, in addition to another bin for the runaway bodies. The evolution of r.m.s. eccentricities and inclinations of the bodies (fragments, planetesimals, and runaway bodies) in each mass bin due to gravitational encounters is calculated using Eqs. (13). Distant encounters between runaway bodies on isolated orbits are also taken into account, following Inaba *et al*. (2001). As to the velocity change caused by gas drag, we use the equations derived by Inaba *et al*. (2001; their Eqs. (27) and (28)) with $C_D = 0.5$, $\rho_{\rm gas} = 1.18 \times 10^{-9}$ g cm^{-3}, and $\eta = 1.85 \times 10^{-3}$. Finally, the effect of inelastic collisions is taken into account following Inaba *et al*. (2001), who calculated collisional dissipation of velocities assuming perfect accretion (Ohtsuki 1992). For such calculations, we use the analytic expression for the collision rate derived by Inaba *et al*. (2001; their Eq. (15)). We also use this expression to evaluate the accretion rate of largest bodies and runaway bodies for given size distributions and calculated velocity distributions.

ACKNOWLEDGMENTS

We thank Satoshi Inaba, Roman Rafikov, and an anonymous referee for their comments on the manuscript, and Larry Esposito for discussions and encouragement. K.O. also thanks Hiroshi Daisaka, Takaaki Takeda, and Hiroyuki Emori for their efforts in the maintenance of computer systems at Tokyo Institute of Technology, where N-body simulations presented here were carried out. This work was supported by the Cassini Project, and part of numerical calculations was performed at the Center for Planning and Information Systems of the Institute of Space and Astronautical Science.

REFERENCES

Greenberg, R., J. F. Wacker, W. K. Hartmann, and C. R. Chapman 1978. Planetesimals to planet: Numerical simulation of collisional evolution. *Icarus* **35**, 1–26.

Greenzweig, Y., and J. J. Lissauer 1990. Accretion rates of protoplanets. *Icarus* **87**, 40–77.

Greenzweig, Y., and J. J. Lissauer 1992. Accretion rates of protoplanets. II. Gaussian distribution of planetesimal velocities. *Icarus* **100**, 440–463.

Hasegawa, M., and K. Nakazawa 1990. Distant encounters between Keplerian particles. *Astron. Astrophys.* **227**, 619–627.

Hénon, M., and J.-M. Petit 1986. Series expansions for encounter-type solutions of Hill's problem. *Celes. Mech.* **38**, 67–100.

Hill, G. W. 1878. Researches in the lunar theory. *Am. J. Math.* **1**, 5–26, 129–147, 245–260.

Hornung, P., R. Pellat, and P. Barge 1985. Thermal velocity equilibrium in the protoplanetary cloud. *Icarus* **64**, 295–307.

Ida, S. 1990. Stirring and dynamical friction rates of planetesimals in the solar gravitational field. *Icarus* **88**, 129–145.

Ida, S., and J. Makino 1992. N-body simulation of gravitational interaction between planetesimals and a planet. I. Velocity distribution of planetesimals. *Icarus* **96**, 107–120.

Ida, S., and J. Makino 1993. Scattering of planetesimals by a protoplanet: Slowing down of runaway growth. *Icarus* **106**, 210–227.

Ida, S., and K. Nakazawa 1989. Collisional probability of planetesimals revolving in the solar gravitational field. III. *Astron. Astrophys.* **224**, 303–315.

Ida, S., E. Kokubo, and J. Makino 1993. The origin of anisotropic velocity dispersion of particles in a disc potential. *Mon. Not. R. Astron. Soc.* **263**, 875–889.

Inaba, S., H. Tanaka, K. Ohtsuki, and K. Nakazawa 1999. High-accuracy statistical simulation of planetary accretion: I. Test of the accuracy by comparison with the solutions to the stochastic coagulation equation. *Earth, Planets, Space* **51**, 205–217.

Inaba, S., H. Tanaka, K. Nakazawa, G. W. Wetherill, and E. Kokubo 2001. High-accuracy statistical simulation of planetary accretion: II. Comparison with N-body simulations. *Icarus* **149**, 235–250.

Kenyon, S. J., and B. C. Bromley 2001. Gravitational stirring in planetary debris disks. *Astron. J.* **121**, 538–551.

Kenyon, S. J., and J. X. Luu 1998. Accretion in the early Kuiper belt. I. Coagulation and velocity evolution. *Astron. J.* **115**, 2136–2160.

Kenyon, S. J., and J. X. Luu 1999. Accretion in the early Kuiper belt. II. Fragmentation. *Astron. J.* **118**, 1101–1119.

Lissauer, J. J., and G. R. Stewart 1993. Growth of planets from planetesimals. In *Protostars & Planets III* (E. H. Levy and J. I. Lunine, Eds.), pp. 1061–1088. Univ. of Arizona Press, Tucson.

Makino, J., M. Taiji, T. Ebisuzaki, and D. Sugimoto 1997. GRAPE-4: A massively-parallel special-purpose computer for collisional N-body simulations. *Astrophys. J.* **480**, 432–446.

Makino, J., T. Fukushige, Y. Funato, and E. Kokubo 1998. On the mass distribution of planetesimals in the early runaway stage. *New Astron.* **3**, 411–417.

Nakagawa, Y., C. Hayashi, and K. Nakazawa 1983. Accumulation of planetesimals in the solar nebula. *Icarus* **54**, 361–376.

Nakazawa, K., and S. Ida 1988. Hill's approximation in the three-body problems. *Prog. Theor. Phys. Suppl.* **96**, 167–174.

Ohtsuki, K. 1992. Evolution of random velocities of planetesimals in the course of accretion. *Icarus* **98**, 20–27.

Ohtsuki, K. 1993. Capture probability of colliding planetesimals: Dynamical constraints on accretion of planets, satellites, and ring particles. *Icarus* **106**, 228–246.

Ohtsuki, K. 1999. Evolution of particle velocity dispersion in a circumplanetary disk due to inelastic collisions and gravitational interactions. *Icarus* **137**, 152–177.

Ohtsuki, K., and H. Emori 2000. Local N-body simulations for the distribution and evolution of particle velocities in planetary rings. *Astron. J.* **119**, 403–416.

Ohtsuki, K., and S. Ida 1998. Planetary rotation by accretion of planetesimals with nonuniform spatial distribution formed by the planet's gravitational perturbation. *Icarus* **131**, 393–420.

Ohtsuki, K., Y. Nakagawa, and K. Nakazawa 1988. Growth of the Earth in nebular gas. *Icarus* **75**, 552–565.

Shiidsuka, K., and S. Ida 1999. Evolution of the velocity dispersion of self-gravitating particles in disc potentials. *Mon. Not. R. Astron. Soc.* **307**, 737–749.

Stewart, G. R., and S. Ida 2000. Velocity evolution of planetesimals: Unified analytical formulas and comparisons with N-body simulations. *Icarus* **143**, 28–44.

Stewart, G. R., and W. M. Kaula 1980. A gravitational kinetic theory for planetesimals. *Icarus* **44**, 154–171.

Stewart, G. R., and G. W. Wetherill 1988. Evolution of planetesimal velocities. *Icarus* **74**, 542–553.

Tanaka, H., and S. Ida 1996. Distribution of planetesimals around a protoplanet in the nebula gas. I. The semi-analytic calculation of the gravitational scattering by a protoplanet. *Icarus* **120**, 371–386.

Tanaka, H., S. Inaba, and K. Nakazawa 1996. Steady-state size distribution for the self-similar collision cascade. *Icarus* **123**, 450–455.

Weidenschilling, S. J. 1989. Stirring of a planetesimal swarm: The role of distant encounters. *Icarus* **80**, 179–188.

Weidenschilling, S. J., D. Spaute, D. R. Davis, F. Marzari, and K. Ohtsuki 1997. Accretional evolution of a planetesimal swarm. 2. The terrestrial zone. *Icarus* **128**, 429–455.

Wetherill, G. W. 1990. Comparison of analytical and physical modeling of planetesimal accumulation. *Icarus* **88**, 336–354.

Wetherill, G. W., and G. R. Stewart 1989. Accumulation of a swarm of small planetesimals. *Icarus* **77**, 330–367.

Wetherill, G. W., and G. R. Stewart 1993. Formation of planetary embryos: Effects of fragmentation, low relative velocity, and independent variation of eccentricity and inclination. *Icarus* **106**, 190–204.